REVIEW

Check for updates

Far-red/NIR BODIPY probes in focus: tailored strategies for organelle-specific imaging and biomedical applications

Charutha Kalarikkal and Chinna Ayya Swamy P [ID] *

Organelles are vital for cellular homeostasis, and their dysfunction is closely linked to various diseases. Consequently, there is growing interest in the development of organelle-targeted probes that facilitate precise diagnosis and therapy while minimizing off-target effects. Fluorescence imaging, particularly utilizing far-red and near-infrared (NIR) fluorophores, has emerged as a potent tool owing to its deep tissue penetration, low background interference, and high spatiotemporal resolution. Among organic fluorophores, BODIPY-based dyes are particularly noteworthy for their excellent photophysical properties and structural tunability. This review highlights recent advancements in the design of far-red/ NIR BODIPY fluorophores engineered for organelle specificity, with a focus on mitochondria, lysosomes, and lipid droplets (LDs). We explore the design strategies, responsive mechanisms, and biomedical applications of these nanoplatforms, while outlining the current challenges and future opportunities. By emphasizing the unique potential of BODIPY scaffolds, this review provides insights into their role in advancing organelle-targeted imaging and theranostics for clinical translation.

1. Introduction

Despite significant technological and biomedical advancements, global health equity remains far from ideal. The COVID-19 pandemic starkly exposed persistent vulnerabilities

Main group Organometallics Optoelectronic Materials and Catalysis lab, Department of Chemistry, National Institute of Technology, Calicut, 673601, India. E-mail: swamy@nitc.ac.in

Charutha Kalarikkal is currently a PhD student under the supervision of Dr Chinna Ayya Swamy P at the National Institute of Technology, Calicut. She received her BS-MS degree from the Indian Institute of Science Education and Research (IISER), Thiruvananthapuram, in 2021. She is a recipient of the prestigious INSPIRE fellowship of the Government of India. Her PhD thesis focuses on the design and synthesis of BODIPY-based NIR fluorophores for the selective localization of organelles, particularly mitochondria, lysosomes, and lipid droplets.

Charutha Kalarikkal

Dr Chinna Ayya Swamy P is an Assistant Professor of Chemistry at the National Institute of Technology, Calicut, India in 2020. He obtained his MSc in General Chemistry from the University of Hyderabad in 2009 and his PhD from the Indian Institute of Science (IISc), Bangalore, in 2014, specializing in main-group organometallics. Following his PhD, he spent five years as a postdoctoral fellow abroad, in the research area of supramolecular and organometallic chemistry. His research focuses on the design and synthesis of novel main-group organometallic optoelectronic materials, solid-state emissive organic fluorophores for OLEDs, bioimaging, and dye-sensitized solar cells (DSSCs), as well as metal-based catalysis and chemosensors for biologically relevant ions.

Chinna Ayya Swamy P

This journal is © The Royal Society of Chemistry 2025

J. Mater. Chem. B, 2025, **13**, 12831–12868 | 12831

within healthcare systems worldwide. Even beyond pandemic-related deaths, non-communicable diseases (NCDs) remain the leading cause of death globally, accounting for approximately 75% of total mortality in 2021.[1] These include cardiovascular diseases (such as heart attacks and strokes), various cancers, chronic respiratory conditions like asthma, and diabetes. Many of these diseases remain incurable, with treatment regimens often extending over decades, placing immense strain on both individual quality of life and global healthcare infrastructure. A major contributing factor to this ongoing crisis is the lack of effective early diagnostic tools and therapeutics that offer high specificity, minimal side effects, and a rapid response rate.[2,3] Conventional drug delivery approaches often fail to overcome the physiological and biochemical barriers within the human body, which limit therapeutic efficacy *via* premature drug degradation, off-target accumulation, and long-term toxicity.[4–6] In response, the scientific community has turned its attention towards advanced drug delivery systems (DDS), particularly subcellular or organelle-specific targeting systems for site-specific therapeutic action.[7–11] Often described as "magic bullets," these precision-guided systems offer the potential to dramatically improve therapeutic outcomes by intervening at the very origin of disease processes, *i.e.*, within the cell.[12]

Every living cell contains a complex and well-organized network of organelles that collectively preserve cellular function and structural integrity. These organelles include both membrane-bound structures, such as the mitochondria, nucleus, endoplasmic reticulum, and lysosomes, and non-membranous entities like nucleoli, stress granules, and Cajal bodies, each fulfilling specialized roles essential for cellular survival.[13–15] This internal compartmentalization ensures that cellular processes occur in parallel without mutual interference, promoting efficiency and rapid adaptation to changing physiological conditions. Rather than operating in isolation, organelles function in a coordinated manner to regulate fundamental biological activities, including energy production, signal transmission, metabolic control, gene expression, and apoptosis.[16] Each of these compartments is characterized by a unique physicochemical environment defined by pH, viscosity, polarity, and the presence of specific biomolecules like enzymes, metal ions, or reactive species.[17] These microenvironments are essential for maintaining the fidelity of cellular signaling and metabolic pathways.[18] Disruption of these environments through genetic mutations, oxidative stress, or metabolic dysfunction can lead to severe pathologies.[19] For example, oxidative stress within mitochondria can lead to excessive generation of reactive oxygen species (ROS), disrupting redox signaling and triggering cell death, a mechanism closely associated with the neurodegenerative diseases such as Parkinson's and Alzheimer's.[20,21] Furthermore, the interdependence of organelles means that malfunction in one often destabilizes others, resulting in systemic cellular dysfunction.[22] This understanding has attracted a growing interest in developing diagnostics and therapeutics that are tailored to specific organelles. Such strategies are becoming central to precision medicine, where spatially targeted interventions within the cell can enhance treatment efficacy while minimizing off-target effects. By enabling localized

drug activation and precise molecular imaging, organelle-targeted approaches offer a powerful solution to the limitations of conventional therapies, holding the potential to transform how we diagnose and treat complex diseases.[23–26]

Bio-imaging technologies have revolutionized diagnostics and disease treatment, with modalities such as magnetic resonance imaging (MRI), positron emission tomography (PET), single-photon emission computed tomography (SPECT), and computed tomography (CT) serving as cornerstones of clinical practice.[27] These techniques offer macroscopic insights into anatomical and functional abnormalities; however, their restrictions, such as limited resolution at the cellular level, dependence on radiotracers, high infrastructure costs, and the potential for damaging sensitive biological structures, hinder their effectiveness in detailed molecular analysis and dynamic biological monitoring.[28] To address these gaps, fluorescence imaging has emerged as a highly promising alternative. Unlike traditional methods, fluorescence imaging enables real-time, non-invasive visualization of molecular interactions and cellular events with high specificity and resolution.[29] It has found widespread utility in applications ranging from cellular mapping to surgical navigation.[30–34] Yet, when operating within the visible (400–700 nm) spectral ranges, fluorescence imaging faces critical challenges, most notably, limited tissue penetration, significant background interference, and photon scattering, all of which constrain its applicability in deep-tissue and whole-body imaging.[34] These drawbacks have fuelled interest in the first near-infrared (NIR-I: 650–950 nm) and second near-infrared region (NIR-II: 1000–1700 nm), where biological transparency is maximized. Fluorophores operating in this window enable significantly deeper penetration, suppressed background auto-fluorescence, and superior spatial resolution ideal for live cell imaging, cancer detection, pharmacokinetic tracking, and therapeutic monitoring.[35] As a result, NIR imaging is rapidly reshaping the landscape of biomedical visualization. A variety of NIR-emissive probes have been developed to date. Inorganic nanostructures like quantum dots, carbon nanotubes, and rare-earth-doped particles offer strong luminescence and stable optical signals. However, their clinical viability is limited by concerns over long-term toxicity, poor degradability, and bioaccumulation in organs such as the liver and spleen.[36] These safety issues have prompted the search for more biocompatible alternatives. Organic small-molecule NIR-fluorophores are increasingly recognized as the next frontier in bioimaging. With advantages such as low immunogenicity, tunable pharmacokinetics, rapid renal clearance, and chemical flexibility, these fluorophores offer a safer platform for *in vivo* imaging.[37] Their structural tunability also allows for the integration of targeting groups, environmental triggers, and therapeutic moieties making them suitable for multifunctional roles in both diagnostics and treatment. The clinical relevance of organic fluorophores is exemplified by the FDA approval of NIR-I dyes such as indocyanine green (ICG) and methylene blue (MB).[35–38] Their successful implementation paves the way for the design of next-generation NIR-I and NIR-II probes, which aim to enhance biocompatibility, imaging performance, and clinical applicability, while offering superior

12832 | *J. Mater. Chem. B*, 2025, **13**, 12831–12868

This journal is © The Royal Society of Chemistry 2025
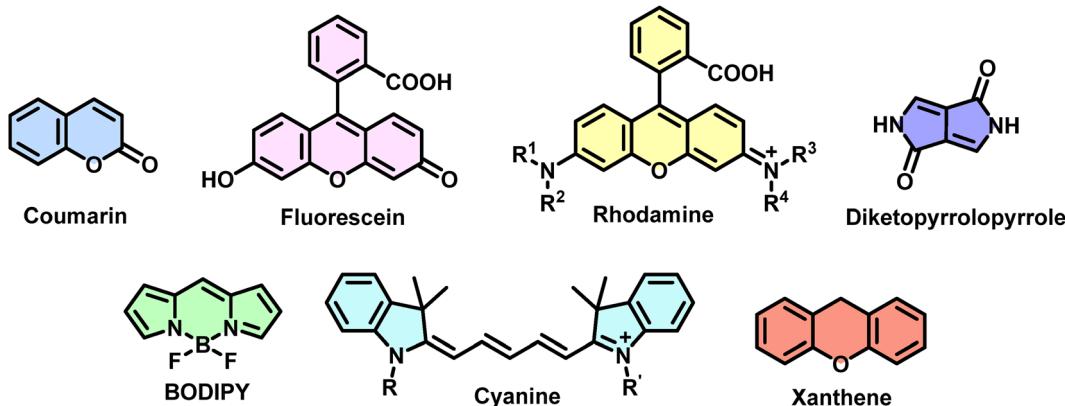
Fig. 1 Common organic fluorophores.

spatial-temporal resolution and sensitivity. Among the various families of organic fluorophores, BODIPY (boron-dipyrromethene) dyes have emerged as standout candidates (Fig. 1). While other dye classes like cyanines suffer from photobleaching, rhodamines from off-target binding, and fluoresceins from poor cellular uptake, BODIPY compounds offer a compelling blend of performance and stability. Key attributes include:

(a) High fluorescence quantum yield (QY)

(b) Low cytotoxicity and high chemical/photostability

(c) Sharp absorption and emission profiles with high molar extinction coefficients.

These traits make BODIPY derivatives a powerful scaffold for crafting advanced probes tailored for organelle-targeted imaging, environmental responsiveness, and theranostic integration.

BODIPY dyes are amenable to structural modifications at the α-, β-, and *meso*-positions, and the $-BF_2$, enabling the design of multifunctional derivatives suitable for a wide array of applications, ranging from photovoltaics and sensors to photodynamic therapy (PDT), photothermal therapy (PTT), and image-guided drug delivery.[40–46] For example, Aza-BODIPYs feature a nitrogen atom replacing the *meso*-carbon. This structural alteration leads to red-shifted absorption and emission, facilitating their use in NIR imaging, despite a modest reduction in QY. These derivatives are widely applied in subcellular visualization, targeted phototherapy, and biomarker detection. Further, commercially available BODIPY probes (*e.g.*, ER-Tracker Green, LysoTracker Red) demonstrate their utility in subcellular imaging.[39,47]

This review provides a focused and up-to-date summary of the fundamental properties of BODIPY dyes, with an emphasis on recent advances in their molecular engineering for NIR applications. We explore core design strategies that have enabled the extension of BODIPY emission into the far-red and NIR spectral regions, which are crucial for deep-tissue imaging, reduced background interference, and enhanced resolution in biological environments. A major theme of this review is the strategic development of organelle-specific BODIPY-based probes. We detail the general principles guiding subcellular targeting, particularly for mitochondria, lysosomes, and lipid droplets (LDs), which are key organelles involved in cellular metabolism, signaling, and disease progression. Special emphasis is placed on

optimizing the photophysical performance, biological compatibility, and target specificity of BODIPY fluorophores, along with a comprehensive discussion of the underlying fluorescence response mechanisms, such as photoinduced electron transfer (PET), intramolecular charge transfer (ICT), Fluorescence resonance energy transfer (FRET), and environmental sensitivity. In addition to their diagnostic capabilities, BODIPY-based fluorophores hold immense promise for therapeutic applications, particularly in phototherapy. We critically evaluate their roles in PDT, PTT, and combinatorial strategies, discussing both *in vitro* and *in vivo* performance, as well as their translational potential in preclinical and clinical contexts. While several reviews have previously explored BODIPY from synthetic and photophysical perspectives, a focused discussion on the design and application of organelle-targeted NIR BODIPY probes remains limited. This review aims to bridge that gap by offering a detailed analysis of both established and emerging approaches for developing BODIPY-based probes tailored for specific subcellular environments and diagnostic or therapeutic functions. Finally, we highlight the latest developments in BODIPY fluorophores that emit in the near-infrared window (NIR-I and NIR-II), emphasizing their superior tissue penetration, reduced autofluorescence, and promise for real-time, non-invasive clinical imaging. Key innovations in NIR-BODIPY molecular design are discussed alongside the challenges that remain for their successful integration into clinical diagnostics. By blending current knowledge and outlining future directions, this review aims to serve as a comprehensive resource for researchers working on long-wavelength BODIPY fluorophores and to support the advancement of precision imaging and targeted therapy through the rational design of organelle-specific fluorescent probes.

1.1 Photophysical modulation and molecular engineering

Since the first report of BODIPY dyes by Treibs and Kreuzer in 1968, BODIPY dyes (4,4-difluoro-4-bora-3*a*,4*a*-diaza-*s*-indacenes) have emerged as a highly versatile class of fluorophores, widely applied in chemical sensing, biomedical diagnostics, and phototherapeutics[48] (Fig. 2). The core structure of BODIPY, characterized by a rigid and largely planar conjugated system, offers an ideal platform for photophysical robustness, including

This journal is © The Royal Society of Chemistry 2025

J. Mater. Chem. B, 2025, **13**, 12831–12868 | **12833**

high molar absorptivity, excellent fluorescence quantum yields, and resistance to photobleaching.[49] Although the boron center may exhibit minor deviations from planarity, the overall geometry supports effective electronic delocalization, enabling predictable optical performance. One of the major strengths of BODIPY dyes lies in their synthetic flexibility. The core structure can be modified at multiple positions using well-established organic reactions such as Suzuki, Sonogashira, and Heck couplings, as well as Knoevenagel condensations, styryl extensions, and nucleophilic substitutions.[50] These modifications enable fine-tuning of both electronic and steric properties. Historically, most native BODIPY dyes fluoresce in the visible spectrum (typically 490–510 nm), which limits their utility in deep-tissue imaging where NIR light is preferable. Nonetheless, their photostability, pH-independence, and minimal background interference make them highly attractive for applications in fluorescence microscopy, including two-photon excitation and live-cell imaging. To unlock their potential in *in vivo* imaging and targeted therapy, significant attention has been directed toward extending BODIPY emission into the far-red and NIR spectral regions through structural modifications such as: styryl substitution (for extended π-conjugation), ring fusion/conformational locking (for rigidity), and Aza-BODIPYs.[51] These strategies yield BODIPY-based fluorophores suitable for multifunctional theranostic applications, including PDT/PTT, fluorescence/photoacoustic dual imaging, and stimuli-responsive drug delivery.[52–55] Despite the substantial progress, several limitations persist that hinder optimal performance in biological systems. A prominent issue is the narrow Stokes' shift characteristic of many BODIPY derivatives, which results in spectral overlap between excitation and emission, leading to self-quenching and decreased imaging resolution. Additionally, hydrophobicity arising from extended π-conjugation often reduces water solubility, limiting their biocompatibility and *in vivo* applicability. Therefore, recent research has focused on overcoming these drawbacks through several traditional and bioengineering methods.

1.2 Traditional design approaches for NIR fluorophores

The development of high-performance NIR fluorophores depends on a set of well-established design principles that aim to optimize their optical properties, biocompatibility, and *in vivo* behavior.[56–58]

1.2.1 Rational structure-based engineering for bathochromic shifts. To achieve NIR absorption and emission, fluorophores are structurally engineered to shift their spectral properties bathochromically. Key strategies include:

(a) Extension of π-conjugation: expanding the π-conjugated framework reduces the highest occupied molecular orbital (HOMO) and lowest unoccupied molecular orbital (LUMO) energy gap, resulting in red-shifted absorption/emission wavelengths.

(b) Donor–Acceptor (D–A) modulation: modifying chemical substituents to enhance electron donor or acceptor features can tune the ICT process. Increasing donor electron density and decreasing acceptor electron density effectively shift emission wavelengths.

(c) Heteroatom incorporation: substituting atoms within the molecular scaffold (*e.g.*, sulfur, nitrogen) can adjust the electronic structure and fine-tune emission profiles.

(d) Aggregate engineering (*e.g.*, J-aggregates): controlling molecular aggregation states, especially the formation of J-aggregates, offers a powerful route to redshift absorption/emission. J-Aggregates, aligned in a head-to-tail fashion, exhibit desirable features such as narrowed Stokes shifts, shortened fluorescence lifetimes, enhanced extinction coefficients, and suitability for *in vivo* imaging applications.

1.2.2 Enhancing probe luminescence. Fluorescence brightness, determined by the product of the molar extinction coefficient and quantum yield (QY), is crucial for high-sensitivity imaging. However, long-wavelength fluorophores are often challenged by non-radiative losses due to vibrational relaxation, π–π stacking, and collisional quenching. Strategies to counteract this include:

(a) Shielding with bulky substituents: introducing sterically hindered side chains reduces solvent interactions and π–π stacking, creating a hydrophobic environment that minimizes nonradiative energy loss.

(b) Rigidification of the molecular framework: incorporating rigid structures or restricting intramolecular motion helps suppress twisted intramolecular charge transfer (TICT) states, enhancing fluorescence output.

(c) Molecular doping and encapsulation: encapsulating fluorophores into amphiphilic polymer matrices or forming aggregates can reduce quenching by physically isolating the dye from quenching agents and restricting molecular motion.

(d) Construction of AIEgens or controlled aggregates: aggregation-induced emission (AIE) fluorophores and controlled
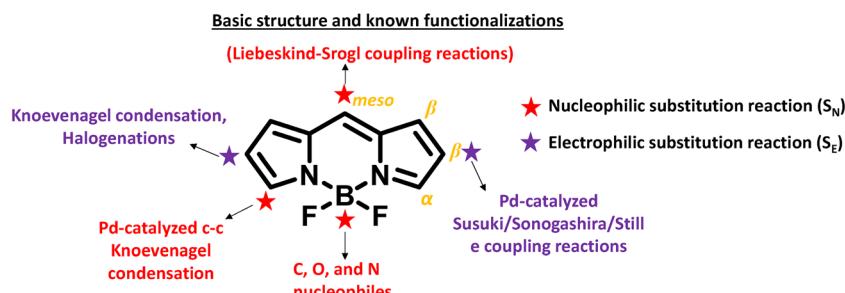

Fig. 2 Basic BODIPY core structure and known functionalization reactions.

12834 | *J. Mater. Chem. B*, 2025, **13**, 12831–12868

This journal is © The Royal Society of Chemistry 2025

J-aggregates can amplify brightness by leveraging restricted intramolecular rotations.

1.3 Emerging bioengineering strategies for NIR fluorophores

Beyond traditional synthetic approaches, recent advancements have explored the integration of biomacromolecules as functional scaffolds or carriers for NIR fluorophores. Encapsulating fluorophores within endogenous or exogenous proteins has demonstrated significant promise by improving brightness and enhancing biocompatibility, such as:[58]

    (i) Serum albumin

    (ii) Fibrinogen

    (iii) Apoferritin

    (iv) β-Lactoglobulin

1.4 Criteria and general strategies for organelle-specific targeting

For effective subcellular imaging and therapeutic intervention, organic fluorescent probes must fulfill several essential criteria:[59–63]

    1. High specificity for the target organelle in live cells and tissues;

    2. Inactivity prior to reaching the target site (to avoid background noise);

    3. Selectivity toward the analyte of interest;

    4. Low cytotoxicity and excellent biocompatibility;

    5. Efficient permeability through both the plasma and organelle membranes;

    6. Cost-effective, synthetically accessible, and stable molecular structure.

Generally, two main approaches are employed for organelle targeting: (1) ligand-based targeting, where probes are covalently conjugated to organelle-localizing motifs or structurally modified to incorporate organelle-specific functionalities; and (2) self-labeling protein/enzyme tags, such as HaloTag7 and SNAP-tag, where a substrate/receptor-bearing probe reacts with the receptor and forms a covalent bond with the protein of interest.[18] While the latter approach offers high specificity, it often limits probe dispersion.

1.5 Fluorescence response mechanisms in organelle-specific probes

Fluorescent probes operate *via* analyte-triggered changes in signal intensity or emission wavelength. The most widely used mechanisms include:[16,34]

    1. Fluorescence resonance energy transfer (FRET): involves non-radiative energy transfer from an excited donor to a ground-state acceptor through dipole–dipole interactions (long-range). This process is efficient when there is significant spectral overlap and a short D–A distance (<100 nm) and is often employed in ratiometric probes for precise quantification of analytes, using cleavable linkers and analyte-responsive chromophores. Here, HOMO and LUMO of the acceptor should be within HOMO and LUMO of the donor.

    2. Photo-induced electron transfer (PET): involves intramolecular electron transfer between a recognition unit and the fluorophore and are of two types: (a) reductive PET (a-PET): electron transfer from donor (recognition group) to fluorophore quenches fluorescence (HOMO of donor lies between HOMO and LUMO of fluorophore), and (b) oxidative PET (d-PET): excited fluorophore donates an electron to an electron-deficient acceptor, also leading to quenching (LUMO of acceptor lies between HOMO and LUMO of fluorophore).

    3. Intramolecular charge transfer (ICT): a push–pull system where donor and acceptor groups are directly attached to the fluorophore. Upon analyte binding, changes in electron distribution modulate the energy gap, leading to red or blue shifts in emission. Specifically, an increase in the electron-withdrawing ability of the fluorophore upon analyte binding reduces the HOMO–LUMO energy gap, resulting in a red shift. In contrast, enhanced electron-donating interactions can increase the energy gap, leading to a blue shift in the emission spectrum. These processes are useful for polarity and pH-sensitive probes and environmental sensors.

These mechanisms enable real-time, high-resolution tracking of dynamic physiological and pathological processes at the subcellular level, especially when coupled with NIR-emitting BODIPY systems. Next, we will be discussing in detail the overview and dynamics of organelles, particularly mitochondria, lysosomes, and lipid droplets (LDs), and the strategic design approaches carried out so far for developing far-red/NIR mitochondrial localized probes. We will also be highlighting the fundamental photophysical properties, detailed mechanisms of action, applicability in biological imaging and therapeutics, and the future perspectives.

2. Mitochondria localized probes

2.1 Overview of mitochondrial dynamics

Beyond their well-known role in ATP production, mitochondria serve as central hubs of cellular metabolism, regulating fatty acid synthesis, calcium homeostasis, ROS generation, and apoptosis.[64–66] Structurally, mitochondria are composed of four key components: the outer mitochondrial membrane (OMM), the inner mitochondrial membrane (IMM), the intermembrane space (IMS), and the matrix. The outer membrane, also referred to as the voltage-dependent anion channel (VDAC), is a lipid bilayer of thickness approximately 60–75 Å. It acts as a barrier between mitochondria and cytoplasm, having numerous porin proteins for the passive diffusion of molecules with a molar mass of less than 5–10 KDa, and can regulate several intracellular signalling pathways.[67,68] The inner membrane is thinner and highly impermeable to most molecules and ions, but it contains several polypeptides. IMM is enriched with lipid cardiolipin, which forms cristae responsible for the wrinkled shape of the inner membrane and helps to enhance the surface area.[65,69] IMM consists of several carrier proteins, oxidoreductases for redox reactions and electron transfer reactions, as well as synthases, thereby promoting key processes such as ATP production and Ca^{2+} homeostasis.[20] Within the IMM lies the mitochondrial matrix, which contains a diverse array of

This journal is © The Royal Society of Chemistry 2025

J. Mater. Chem. B, 2025, **13**, 12831–12868 | **12835**

enzymes, proteins, and mitochondrial DNA crucial for metabolic functions. The IMS, located between the OMM and IMM, is the smallest and most constricted compartment, yet it plays an essential role in modulating various cellular processes.[20,67–69] Mitochondria are also dynamic and heterogeneous organelles within the same cell. They continually undergo processes such as fission, fusion, mitophagy, and mitochondrial transport, all of which are vital for maintaining their normal functions. These dynamic behaviors influence mitochondrial number, size, shape, plasticity, and distribution.[20] Given their critical role in fundamental cellular activities, mitochondrial dysfunctions are closely associated with numerous diseases, such as cancer, neurodegenerative diseases, cardiovascular disorders, autoimmune responses, and aging. Thus, mitochondria can be considered as potential biomarkers for early diagnosis, treatment, and prognosis of diseases such as cancer.[20] Nevertheless, many aspects of the fundamental processes and mechanisms of action, as well as the intricate relationship between mitochondrial structure and dynamics in both healthy and diseased states, remain unclear and require urgent focus, especially since they ultimately determine the cell's fate. Needless to say, it is essential to develop mitochondria-targeted fluorescent probes enabling non-invasive, real-time monitoring of their dynamics with high resolution, sensitivity, and specificity.

2.2 General design rules for mitochondrial probes

During the mitochondrial oxidative phosphorylation and Krebs cycle processes, the proton pumps on the IMM may transport protons from the matrix to the IMS, which results in a highly negative membrane potential (150–180 mV) compared to aqueous plasma membrane potential (30–40 mV). This might increase the cation concentration in the matrix by 100–1000-fold when compared to cytosol (3–5-fold).[18] Therefore, the basic principle for mitochondrial probe design is to have cations with strong lipophilicity, so that they can diffuse through the phospholipid bilayer and accumulate on the matrix when compared to other organelles.

1. Lipophilic cations as mitochondrial targeting moieties: intrinsic lipophilic cationic probes such as rhodamine, cyanine, and indole are widely known for their mitochondrial targeting ability by electrostatic interaction, and some of them are even commercialized, such as MitoTracker Green (MTG), MitoTracker Orange (MTO), MitoTracker Red (MTR), MitoTracker Deep Red (MTDR) probes. Although the benzyl chloride groups in these commercial probes form covalent bonds with mitochondrial proteins for long-term labelling, they exhibit significant drawbacks. These include cytotoxicity due to respiration inhibitory activity and low photostability, which are crucial for super-resolution imaging techniques such as stimulated emission depletion (STED) imaging which requires high intensity laser source for ultra resolution.[70]

2. Post-lipophilic cation functionalization of neutral fluorophores: BODIPY fluorophores which exhibit excellent optical properties such as high molar extinction coefficient, high quantum yield, low cytotoxicity and high photostability are neutral probes which won't show preferential mitochondrial imaging applicability. In such scenarios, researchers started to introduce post-functionalized lipophilic cationic groups into the neutral probes so that they can specifically target the mitochondria. For example, triphenyl phosphonium salt (TPP$^+$) with three lipophilic phenyl groups can easily diffuse through the mitochondrial membranes and can accumulate in the matrix.[16,64]

3. Labelling peptides and transport proteins: additionally, natural and synthetic peptides having either cationic (arginine, lysine) or hydrophobic (phenylalanine, cyclohexylalanine) moieties, as well as mitochondrial transport proteins, have also been utilized for specific targeting. Multiple positive charges ensure the lipophilicity, hydrophilicity, and biocompatibility of probes. However, the cationic groups can sometimes disrupt the membrane potential, thereby leading to membrane rupture and cell death. Therefore, it is significant to develop novel biocompatible mitochondrial tags with outstanding imaging performance by optimizing the design approach.[18]

2.3 Chemical routes to far-red/NIR mitochondrial labelling probes and their applicability

Ideally, the organelle-specific fluorescent probe should have a fluorophore covalently linked to an organelle-specific targeting moiety, which drives the probe to the target site, and a response unit that changes the fluorescence signal upon interaction with the analyte of interest. The rational design approaches for mitochondrial imaging demand careful consideration of both cellular and probe-specific parameters.[59] A summary of the photophysical properties of mitochondrial NIR BODIPY probes is given in Table 1.

Exploiting these insights, a variety of BODIPY-based NIR fluorescent probes have been developed for precise mitochondrial labelling. Peng et al. synthesized a water-soluble, cationic NIR probe 1 by introducing phenyl and thienyl groups at the 3,5-positions and 1,7-positions, respectively, and a quaternized pyridyl group at the 8-meso position (Fig. 3).[71] The phenyl and thiophene groups enhanced π-conjugation and reduced steric hindrance to improve vibrational flexibility, while the quaternized pyridyl group enabled mitochondrial-specific targeting ability. Probe 1 showed excellent photostability, low cytotoxicity, moderate quantum yield, a large Stokes' shift (>40 nm), and was insensitive to solvent polarity and pH. Notably, the probe allowed the monitoring of mitochondrial swelling during cellular damage in a membrane potential-independent manner.

Despite the advancements, the highly dynamic and complex morphology with a small size makes the probes difficult to travel throughout the mitochondrial compartments. Particularly, challenges remain in visualizing fine mitochondrial structures such as cristae, which are below the resolution limits of conventional microscopy due to their small dimensions (<100 nm spacing). Addressing this, in 2021, Jiang et al. developed a fluorescent BODIPY probe 2b, which enabled visualization of morphology and cristae of mitochondria using ultra-high-resolution microscopy via Knoevenagel condensation of 4-dimethylaminobenzaldehyde at the 3,5-positions of BODIPY to extend π-conjugation and introduced a TPP moiety for mitochondrial targeting (Fig. 3).[72] The probe 2b, having a

12836 | J. Mater. Chem. B, 2025, 13, 12831–12868

This journal is © The Royal Society of Chemistry 2025

Table 1 Summary of photophysical properties of Mitochondrial NIR BODIPY probes
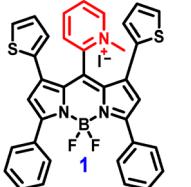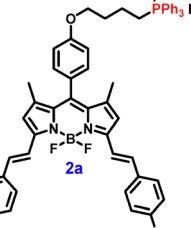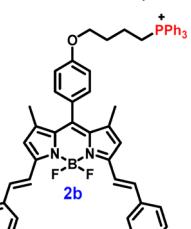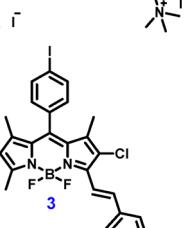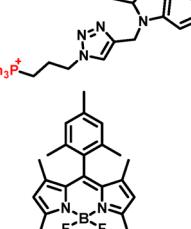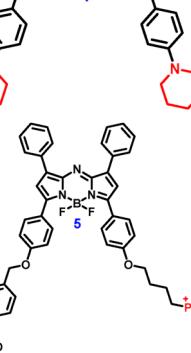
| Probes (P)	Analytes	Solvent	$\lambda_{ex}/\lambda_{em}$ (nm)	QY (ϕ_F)	Probe Conc/ dynamic range (μM)	LOD	Comments	Ref.
1	—	ACN	670/718	0.31	—	—	Pyridyl probe for membrane potential independent mitochondrial imaging	71
2a	—	H₂O DMSO	717/− 705/760	0.03	—	—	Not suitable for imaging due to aggregation caused quenching (ACQ) in water	72
2b	—	H₂O	617/630	0.43	—	—	TPP probe for high resolution mitochondrial imaging- alternative to Mito tracker red	72
3	—	EtOH	612/650	0.4	—	—	TPP probe for- mitochondrial imaging	73
4	—	ACN	681/751	0.04	—	—	Piperidinyl probe for mitochondrial imaging	74
5	H₂O₂	PBS (pH 7.4, 0.01 M)	700/730	P: 0.007 P·H₂O₂: 0.40	10 μM/0–100 μM	23 nM	Turn-on probe; real-time H₂O₂ detection in cells and pulmonary fibrosis mice models; mitochondrial imaging	75

This journal is © The Royal Society of Chemistry 2025
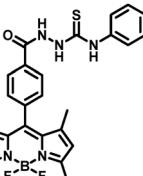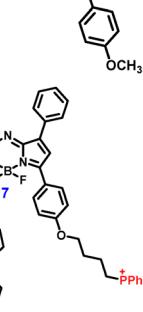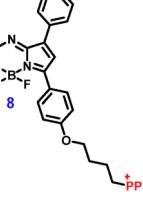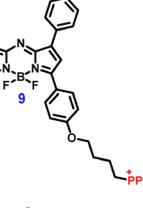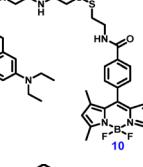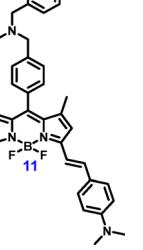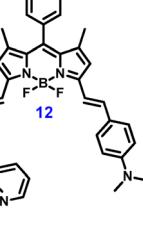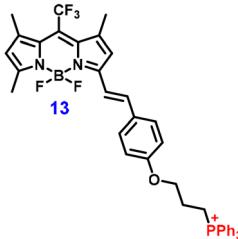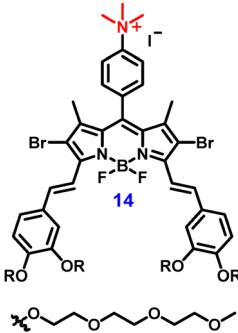
J. Mater. Chem. B, 2025, **13**, 12831–12868 | **12837**

Table 1 (*continued*)

Probes (P)	Analytes	Solvent	$\lambda_{ex}/\lambda_{em}$ (nm)	QY (ϕ_F)	Probe Conc/ dynamic range (μM)	LOD	Comments	Ref.
6	ClO⁻	H₂O/THF (1/1, v/v pH 7.4)	590, 642/ 595, 665	P_{665}: 0.44 P·ClO$_{665}^-$: 0.42	10 μM/0–70 μM	1.15 μM	Ratiometric probe; mitochondrial probe for ClO⁻ detection in living cells	76
7	HNO	HEPES buffer (0.01 M, pH 7.4)	680/730	—	2 μM/0–10 μM	50 nM	Turn-on probe; mitochondrial imaging of anti-inflammatory effects of HNO in cell model and rat model of gouty arthritis	77
8	Na₂S₂	HEPES buffer (0.01 M, pH 7.4, 0.5% DMSO, 0.5% TW 80)	675/730	—	10 μM/0–10 μM	25 nM	Turn-on probe; mitochondrial H₂S$_n$ imaging in cells and *in vivo*	78
9	Na₂S₄	HEPES buffer (0.01 M, pH 7.4, 0.5% DMSO, 0.5% TW 80)	680/720	—	10 μM/0–10 μM	3.1 nM	Turn-on probe; sulfane sulfur detection in live cells and *in vivo* under hypoxia stress; mitochondrial imaging	79
10	GSH	EtOH/PBS buffer (1:2 v/v, 20 mM, pH 7.4)	480/512, 656	—	5 μM/10–100 μM	0.26 μM	Ratiometric probe; mitochondrial bithiol detection in living cells	80
11	Cu²⁺	Mouse blood serum/H₂O (1:10, v/v)	720/784	—	2 μM/0.45– 36.30 μM	—	Turn-off probe; Cu²⁺ sensor in blood serum; Cu²⁺ sensor in live cells and image mitochondria	81
12	Hg²⁺	ACN/HEPES buffer (3:7 v/v, 10 mM, pH 7.2)	620/650	P: 0.026 P·Hg²⁺: 0.12	2 μM/0–150 μM	0.17 μM	Turn-on probe; detection of Hg²⁺ ion in the mitochondria of the live Hct116 cells	82

12838 | *J. Mater. Chem. B*, 2025, **13**, 12831–12868

This journal is © The Royal Society of Chemistry 2025

Table 1 (continued)

Probes (P)	Analytes	Solvent	$\lambda_{ex}/\lambda_{em}$ (nm)	QY (ϕ_F)	Probe Conc/ dynamic range (μM)	LOD	Comments	Ref.
13	Viscosity	Glycerol/H₂O mixtures	610/657	P_{water}: 0 $P_{glycerol}$: 0.19	2 μM/1–950 cP	0.48 cP	Turn-on probe; mitochondrial imaging of cellular viscosity	83
14	—	MeOH	671/709	0.06	—	—	¹O₂ mediated PDT; mitochondrial imaging IC₅₀ (dark): 98.97 ± 0.50 μM (HeLa), 99.13 ± 0.35 μM (MCF-7) IC₅₀ (light): 0.130 μM (HeLa), 0.058 μM (MCF-7)	84

quaternary ammonium group, efficiently penetrated cellular and mitochondrial membranes due to the negative membrane potential. They also tried to understand the significance of hydrophilicity in membrane permeability by synthesizing a completely hydrophobic **2a** probe that aggregated in aqueous media, leading to aggregation-caused quenching (ACQ) and poor cell permeability, limiting its use in mitochondrial imaging. The probe **2b** displayed excellent biocompatibility, photostability, and chemical stability, making it a promising alternative to commercial MitoTracker Red, which suffers from photobleaching and phototoxicity after 30 minutes of laser irradiation (Fig. 4A).

Compared to one-photon NIR emitters, two-photon excitable NIR probes offer deeper tissue penetration, higher resolution, and reduced photobleaching and photodamage. With this in mind, Belfield et al. designed a red two-photon probe **3** with carbazole groups at the 3,5-positions via a Knoevenagel condensation to extend the π-conjugation while maintaining the intrinsic optical properties of the BODIPY core (Fig. 3).[73] A TPP moiety optimizes hydrophilic-lipophilic balance for targeted mitochondrial localization. Additionally, the aryl iodo group at the meso position allows further functionalization to extend conjugation and shift emission into the NIR region. Probe **3** also demonstrated excellent photostability, low cytotoxicity, and resistance to solvent polarity effects (Fig. 4B).

While cationic probes remain widely used for mitochondrial imaging, their limitations, such as susceptibility to changes in membrane potential, nonspecific diffusion, and potential cytotoxicity during long-term imaging, necessitate alternative strategies. In response, Xu et al. synthesized a neutral NIR probe **4** having piperidinyl groups for mitochondrial targeting via

Knoevenagel condensation at the 3,5-positions of BODIPY core (Fig. 3).[74] Probe **4** exhibited excellent biocompatibility, low cytotoxicity, high photostability, and selective mitochondrial staining.

2.4 Chemical routes to far-red/NIR mitochondrial biosensing probes and their applicability

Mitochondria act as key sources of bioactive molecules, including reactive oxygen, nitrogen, and sulfur species (RONSS), which play vital roles in regulating a wide range of physiological and pathological functions. Owing to their dynamic distribution between different subcellular compartments, real-time, in situ monitoring of RONSS within mitochondria requires sensitive, selective, and organelle-specific fluorescent probes. Among many classes of mitochondrial biosensors, far-red/NIR BODIPY-based fluorescent probes have attracted considerable interest due to their desirable photophysical properties, such as high photostability, deep tissue penetration, low background autofluorescence, and minimal phototoxicity. The following subsections detail recent advances in BODIPY-based NIR probes tailored for the selective detection of key mitochondrial analytes such as hydrogen peroxide (H_2O_2), hypochlorite (ClO^-), nitroxyl (HNO), RSS, metal ions, microenvironmental viscosity, and evaluate their sensing mechanisms, targeting strategies, and biomedical applicability.

2.4.1 Detection of H_2O_2 in mitochondria. Among ROS, H_2O_2 is important for cellular signaling, intracellular redox balance, and interactions with essential biomolecules like DNA, proteins, enzymes, and lipids. Abnormal levels of H_2O_2 can disrupt normal biological processes and have been associated with various diseases, such as lung injury, cardiovascular disorders, diabetes, neurodegenerative conditions, and cancer.

This journal is © The Royal Society of Chemistry 2025

J. Mater. Chem. B, 2025, **13**, 12831–12868 | **12839**
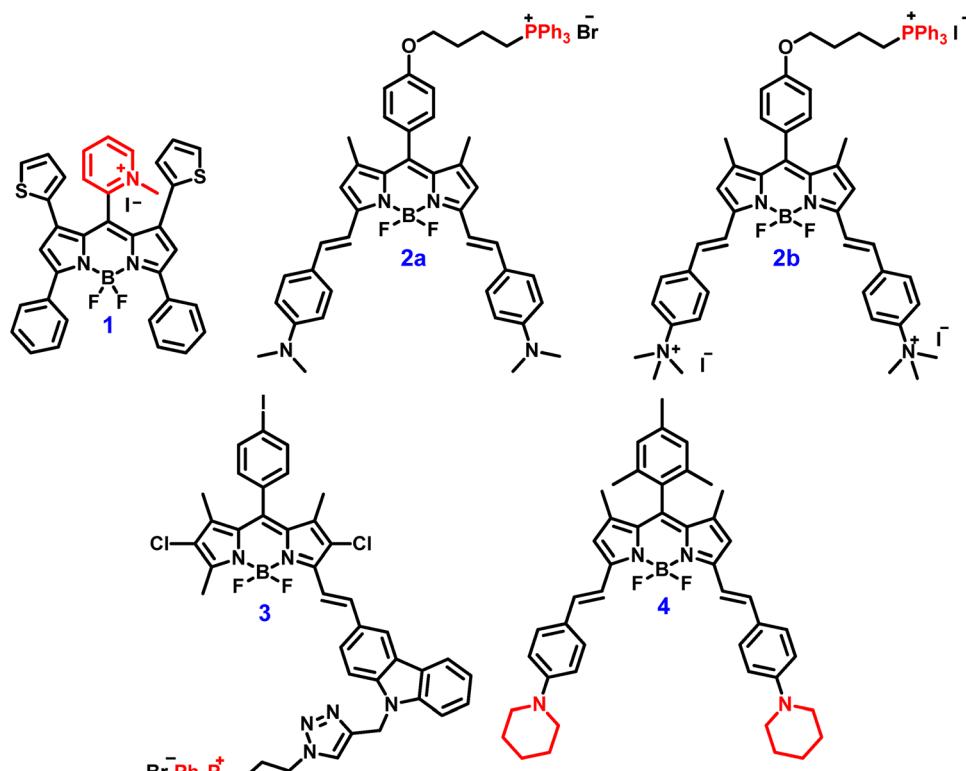
Fig. 3 Chemical structures of probes **1–4**. (Redrawn the ChemDraw structures from ref. 71–74).
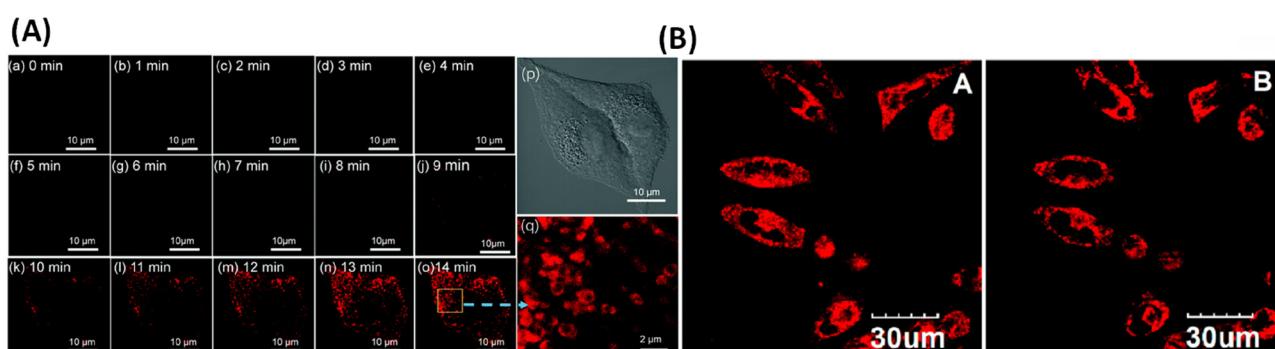

Fig. 4 (A) Rapid cellular uptake and super-resolution images of probe **2** over time (0–14 min) under 405 nm excitation beam. Reproduced with permission from ref. 72, Copyright 2021 Royal Society of Chemistry. (B) Similar one-photon-A (λ_{ex} = 559 nm, λ_{em} = 600–660 nm) and two-photon-B images (λ_{ex} = 900 nm, λ_{em} = 600–660 nm) of probe **3** in MCF-7 cells. Reproduced with permission from ref. 73, Copyright 2013 American Chemical Society.

In 2021, Yu *et al.* developed a mitochondria-targeted NIR fluorescent probe **5** based on Aza-BODIPY for monitoring intracellular H_2O_2 levels in living cells (A549 and PC9 models) and in a mouse model of bleomycin-induced pulmonary fibrosis (Fig. 5, 8A and 12).[75] The design strategy involved: (a) using an activatable Aza-BODIPY fluorophore that offers NIR emission, high photostability, and low cytotoxicity; (b) incorporating 4-bromomethylphenylboronic acid pinacol ester as the H_2O_2 recognition unit; and (c) attaching a lipophilic TPP$^+$ cation to target mitochondria. The detection mechanism relies on a fluorescence "off–on" response in the presence of H_2O_2. H_2O_2 triggers oxidation and cleavage of the boronate group, which

hinders the PET from the excited fluorophore to the recognition moiety, thereby restoring fluorescence. Probe **5** showed excellent selectivity, a low detection limit (below 0.1 μM), and strong photostability. Further studies on pulmonary fibrosis mice models revealed that oxidative stress caused by increased H_2O_2 levels is linked to disease progression. Inhibiting NADPH oxidase 4 (NOX4), helped reduce this progression, highlighting the potential of this probe not only for detection but also as part of an innovative therapeutic strategy for pulmonary fibrosis.

2.4.2 Detection of ClO$^-$ in mitochondria. Qian *et al.* engineered a BODIPY-based fluorescent probe **6** designed specifically for detecting hypochlorous acid (HClO) or hypochlorite

12840 | *J. Mater. Chem. B*, 2025, **13**, 12831–12868

This journal is © The Royal Society of Chemistry 2025
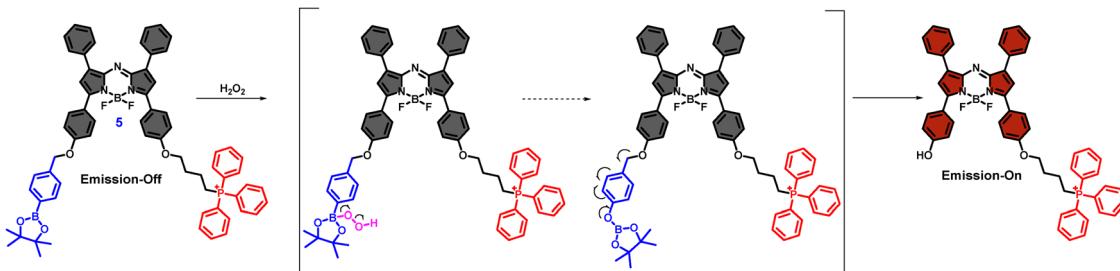
Fig. 5 Turn on mechanism of NIR mitochondrial probe **5** for H$_2$O$_2$ detection. (Redrawn the ChemDraw structures from ref. 75).

(ClO$^-$), a ROS crucial for immune defense and bacterial disinfection (Fig. 6, 8B and 12).[76] To achieve NIR emission, anisic aldehyde was conjugated to the 3,5-positions of the BODIPY core, enhancing π-conjugation. The probe **6** features a thiosemicarbazide group as the recognition unit, chosen for its high sensitivity and selectivity toward ClO$^-$ through a desulfurization reaction. When exposed to ClO$^-$, thiosemicarbazide undergoes desulfurization, forming an electron-withdrawing 1,3,4-oxadiazole, which delocalizes some of the π-electron density from the BODIPY core and quenches its fluorescence. The probe **6** displayed two emission peaks at 595 nm and 665 nm, which responded differently to HOCl: the emission peak intensity at 595 nm increased, while the peak at 665 nm decreased, with minimal interference from other ROS or biological ions. This shift can be seen visually as a color change. The fluorescence intensity ratio (I_{595nm}/I_{665nm}) correlates linearly with HOCl concentrations from 0 to 70 μM, with a detection limit as low as 1.15 μM, and the probe remained stable across a pH range of 6.86 to 11.79. Furthermore, the probe **6** exhibited two-photon absorption properties-when excited at 800 nm, its emission peak red-shifted from 656 nm to 688 nm, with a 32-fold enhancement in emission intensity upon ClO$^-$ exposure. This highly specific ClO$^-$ sensor has also been successfully used for imaging HOCl in mitochondria.

2.4.3 Detection of HNO in mitochondria. Recently, there has been growing interest among researchers in accurately and rapidly detecting endogenous nitroxyl (HNO) in living systems,


Fig. 6 Ratiometric detection mechanism of NIR mitochondrial probe **6** for OCl$^-$. Reproduced with permission from ref. 76, Copyright 2017 Royal Society of Chemistry.

due to its significant role in various physiological functions, especially its pharmacological and anti-inflammatory effects. However, studying endogenous HNO production in mitochondria remains challenging because of its rapid conversion to nitrous oxide (N$_2$O) through dimerization and dehydration, as well as the complexity of biological environments. To address this, Chen et al. developed a NIR fluorescent probe **7** for real-time, in situ monitoring of endogenous HNO from the reaction between nitric oxide (NO) and hydrogen sulfide (H$_2$S) within the mitochondria of live cells and rat models (Fig. 7, 8C and 12).[77] The probe **7** features an Aza-BODIPY fluorophore, a diphenylphosphinobenzoyl group that responds to HNO, and a TPP$^+$ moiety for targeting mitochondria. Its detection mechanism involves the Staudinger ligation between triarylphosphine and HNO, producing a phosphine oxide and aza-ylide intermediate. This intermediate then undergoes a fast intramolecular ester aminolysis and release of the probe, which triggers fluorescence "turn-on". They also confirmed the endogenous generation of polysulfides (H$_2$S$_n$) during this biosynthetic pathway by using a probe Cy-Mito, highlighting the cross-talk between reactive nitrogen species (RNS) and reactive sulfur (RSS) species in biological systems. Probe **7** demonstrated excellent sensitivity with a detection limit of 50 nM, strong selectivity for HNO even in the presence of other biological molecules, low toxicity, and high photostability. Further, probe **7** can be utilized for visualizing the anti-inflammatory function of endogenous HNO in both cellular and rat models of gouty arthritis.

2.4.4 Detection of RSS in mitochondria: sulfane sulfur species. Chen and his team developed a mitochondria-targeted NIR fluorescent probe **8** to detect H$_2$S$_n$ (polysulfide species), which are redox-active forms of H$_2$S that may play a key role in intracellular redox signaling (Fig. 9, 12, 14A and B).[78] The probe **8** was effective in identifying both externally supplied and endogenously produced H$_2$S$_n$ in living RAW264.7 cells and in vivo mice models. Their design strategy includes (a) an aza-BODIPY fluorophore for NIR emission with "on–off" fluorescence response, (b) a nitro-activated fluorobenzoate group as the response site having a bis-electrophilic center for high reactivity, and (c) a lipophilic TPP$^+$ moiety for mitochondrial targeting. The strong electron-withdrawing nitro-activated fluorobenzoate moiety promotes a d-PET from the excited fluorophore to the recognition group, resulting in a fluorescence "off" state. In the presence of H$_2$S$_n$ (H$_2$S$_2$ as a model compound), this d-PET process is interrupted. H$_2$S$_n$ reacts through a nucleophilic aromatic substitution (SNAr), replacing the fluorine atom and forming an intermediate
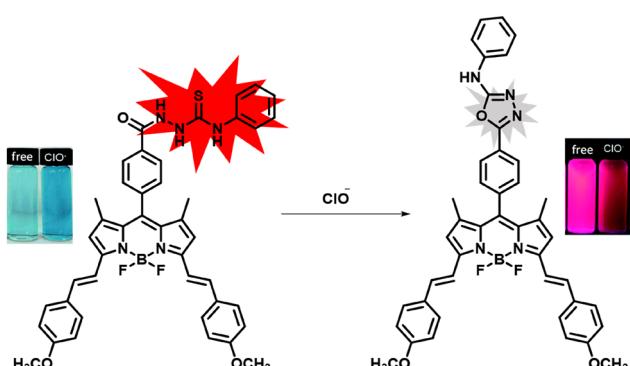
This journal is © The Royal Society of Chemistry 2025

J. Mater. Chem. B, 2025, **13**, 12831–12868 | **12841**
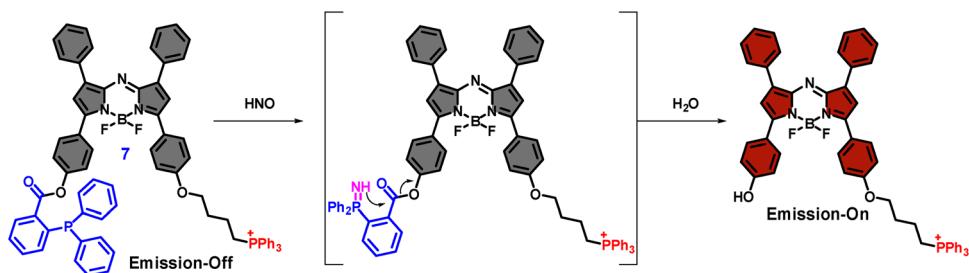
Fig. 7 Turn on mechanism of NIR mitochondrial probe **7** for HNO detection. (Redrawn the ChemDraw structures from ref. 77).
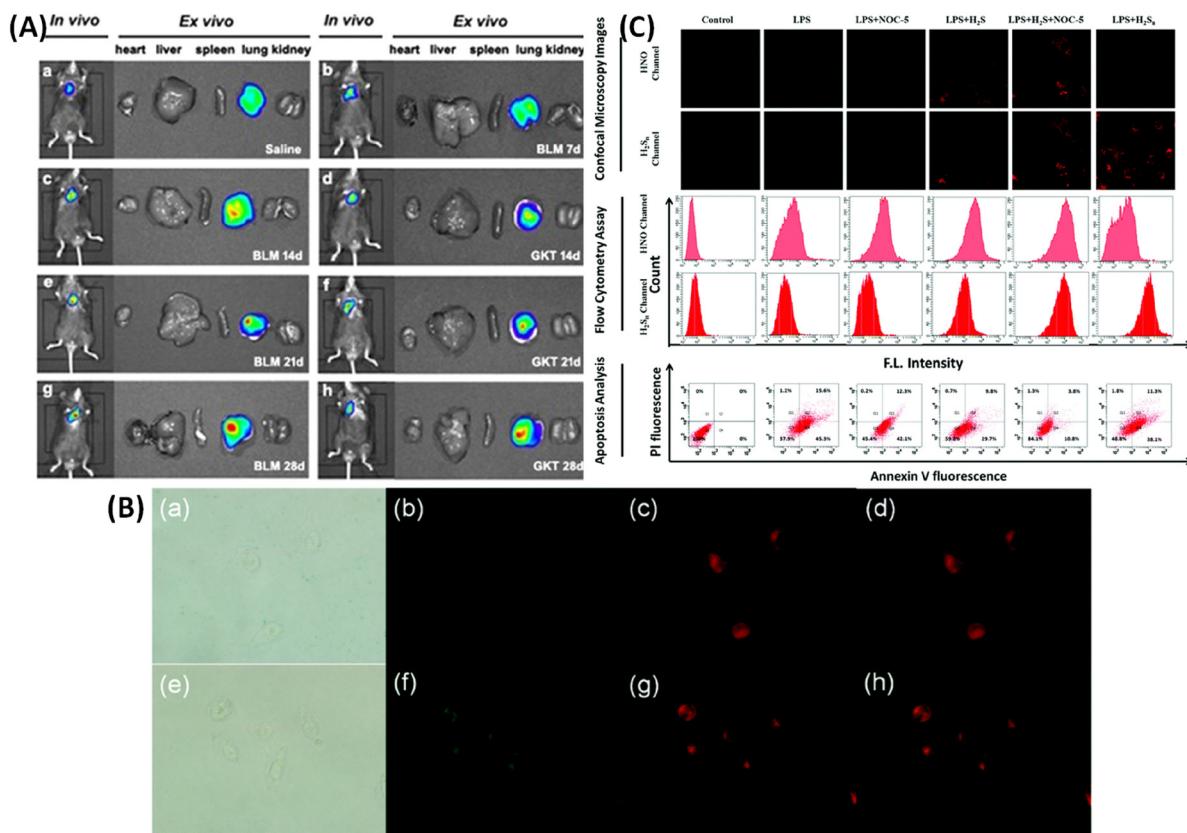

Fig. 8 (A) Fluorescence imaging (*in vivo* and isolated organs of probe **5**) of H_2O_2 level in bleomycin-induced pulmonary fibrosis bleomycin mice models. Reproduced with permission from ref. 75, Copyright 2021 American Chemical Society. (B) Confocal imaging of probe **6** with ClO^- and mito in different channels (two-photon imaging): (a) and (e)-bright field, (b) and (f)-green channel, (c) and (g)-red channel, (d) and (h)-yellow-green channel. Reproduced with permission from ref. 76, Copyright 2017 Royal Society of Chemistry. (C) Fluorescence images, flow cytometry assay, and apoptosis analysis of probe **7** in an inflammatory cell model system for HNO and H_2S_n detection where Q1–Q4 stands for necrotic, late apoptosis, viable, and early apoptosis respectively. Reproduced with permission from ref. 77, Copyright 2019 Royal Society of Chemistry.

with a free thiol (–SH) group. This intermediate further undergoes intramolecular cyclization with the ester moiety, ultimately releasing the fluorophore and restoring fluorescence ("on" state). Remarkably, probe **8** exhibited a 24-fold increase in fluorescence intensity within 30 s, making it well-suited for real-time monitoring of H_2S_n, which are known for their rapid metabolism and fluctuating concentrations. Probe **8** demonstrated high specificity for H_2S_n and was unreactive to other biologically relevant RONSS and biological thiols. This probe holds potential for uncovering biological mechanisms and understanding the physiological and pathological roles of H_2S_n in various signaling pathways.

The same research team explored the relationship between sulfane sulfur and ROS under hypoxic conditions, given that sulfane sulfur is known for its antioxidant roles in biological systems. They designed an activatable NIR Aza-BODIPY probe **9**, functionalized with TPP^+ for targeted mitochondrial imaging and phenyl selenol (pK_a 5.9) as the sulfane sulfur-responsive unit due to its higher electrophilicity compared to the thiophenol (–SH) group (pK_a 6.5) (Fig. 10 and 12).[79] The detection mechanism was based on the tautomerization of sulfane sulfur into a thiosulfoxide form. Due to the weak thiosulfoxide bond, it readily transfers active sulfur to a suitable acceptor, in this

12842 | *J. Mater. Chem. B*, 2025, **13**, 12831–12868

This journal is © The Royal Society of Chemistry 2025
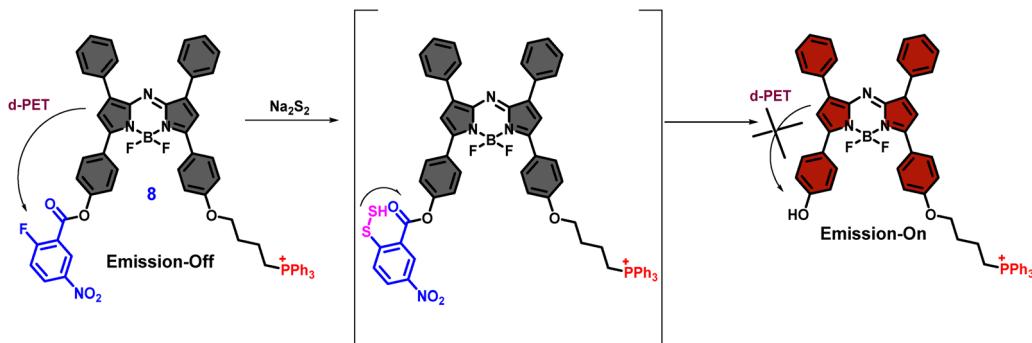
Fig. 9 Proposed mechanism of NIR mitochondrial probe **8** for H_2S_n detection. (Redrawn the ChemDraw structures from ref. 78).
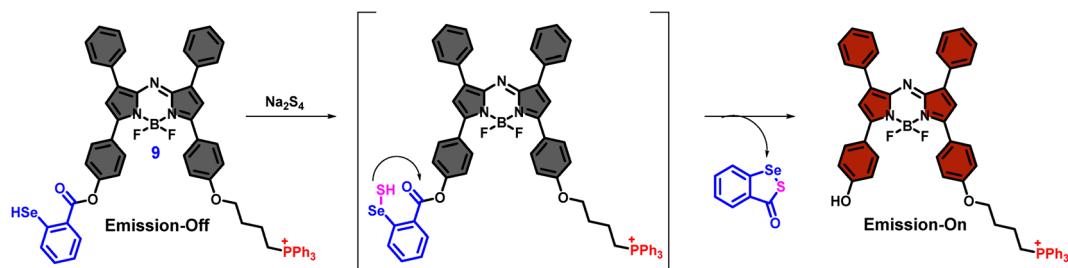

Fig. 10 Proposed mechanism of NIR mitochondrial probe **9** for sulfane sulfur detection. (Redrawn the ChemDraw structures from ref. 79).

case, phenyl selenol, forming a –Se–SH adduct. This intermediate then undergoes intramolecular cyclization with the ester, triggering the release of the fluorophore and switching the probe to its "on" state. Probe **9** demonstrated excellent sensitivity and selectivity, with a low detection limit of 3.1 nM. Probe **9** showed both qualitative and quantitative monitoring of sulfane sulfur species under hypoxic stress in live cells and *in vivo*. Additionally, they exhibited high specificity for sulfane sulfur over other reactive sulfur species and good stability under various physiological conditions. The authors suggested that sulfane sulfur production is closely related to hypoxia progression and contributes to cellular protection by scavenging ROS during hypoxia-induced oxidative stress *via* inhibiting caspase-dependent apoptosis.

2.4.5 Detection of RSS in mitochondria: bithiols. Biological thiols, including cysteine (Cys), homocysteine (Hcy), and glutathione (GSH), play crucial roles in regulating normal physiological functions, especially in maintaining redox balance and metabolic processes. Any disruption in their levels can lead to various diseases. Recently, Liu and his colleagues introduced a new ratiometric NIR fluorescent probe **10** based on FRET (Fig. 11, 12 and 14C).[80] The probe **10** consists of a BODIPY donor and a rhodamine acceptor connected by disulfide bonds for intracellular thiol detection. Upon excitation at 480 nm (BODIPY donor), the probe showed a strong rhodamine emission signal at 656 nm and a weak BODIPY signal at 512 nm, attributed to efficient FRET with approximately 94% energy transfer efficiency. When GSH levels increase, the NIR emission
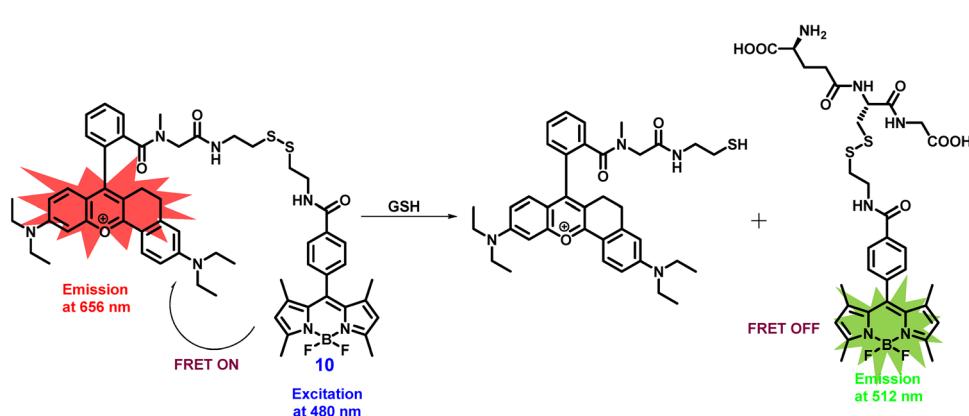

Fig. 11 Proposed ratiometric detection mechanism of probe **10** to bithiols. (Redrawn the ChemDraw structures from ref. 80).

This journal is © The Royal Society of Chemistry 2025

J. Mater. Chem. B, 2025, **13**, 12831–12868 | **12843**
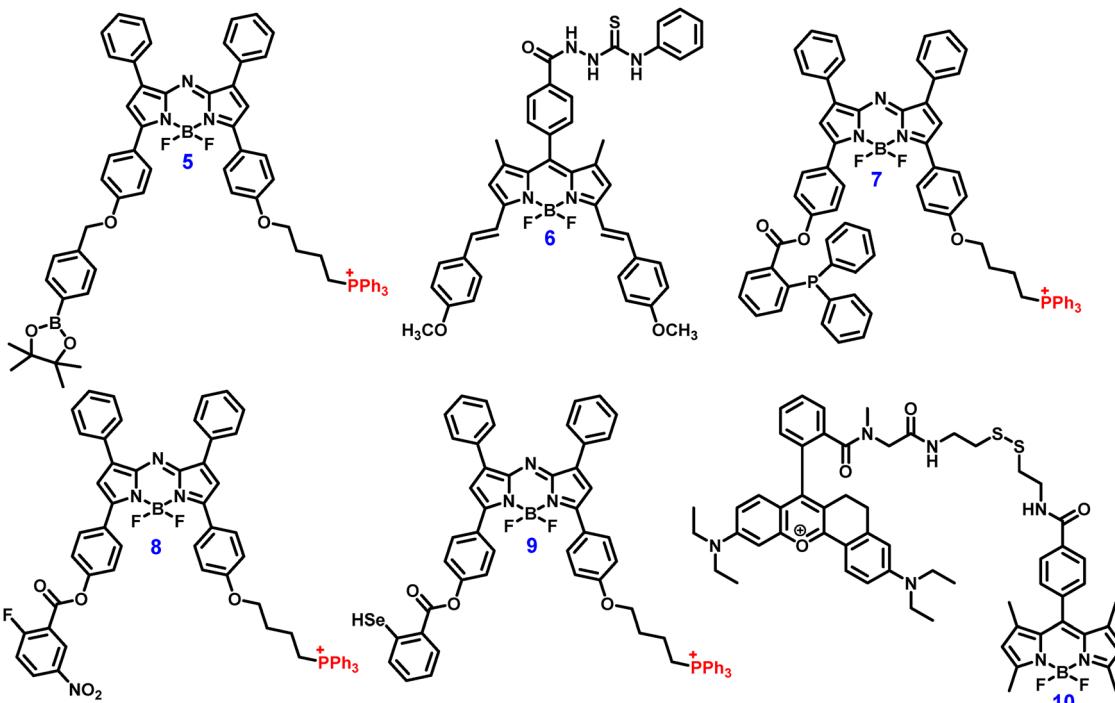
Fig. 12 Chemical structures of probes **5–10**. (Redrawn the ChemDraw structures from ref. 75–80).

diminishes while the BODIPY signal intensifies due to FRET disruption caused by disulfide bond cleavage. Probe **10** demonstrated excellent sensitivity for GSH, with a detection limit of 0.26 μM, high selectivity over other competing species, and pH stability. Cellular imaging studies confirmed the mitochondria-specific imaging and bithiol detection in living HeLa cells.

Compared to probes **8** and **9**, which rely mainly on a turn-on mechanism, probe **10** provides a ratiometric response, thereby minimizing systematic errors associated with single-wavelength probes and enabling quantitative analysis of thiol.

2.4.6 Detection of ions in mitochondria. In addition to reactive species, dysregulated metal ion concentrations can perturb mitochondrial function. Chen *et al.* reported a NIR

BODIPY-based "turn-off" fluorescent probe **11** incorporating a di(pyridylmethyl)amine (DPA) recognition unit for Cu^{2+} ion detection (Fig. 13).[81] The probe **11** was synthesized by the condensation reaction between 4-*N*,*N*-dimethylaminobenzaldehyde and 8-[di(2-picolyl)amine-4-benzyl]-substituted BODIPY core. The emission peak at 765 nm was quenched upon binding with Cu^{2+} ions, when excited at 704 nm, due to the PET mechanism. Interestingly, probe **11** also exhibited increased fluorescence upon interaction with Mn^{2+} ions, attributed to aggregate formation. It showed minimal interference from other metal ions, indicating high selectivity. Additionally, the probe **11** specifically targeted mitochondria and can serve as a fluorescence sensor for Cu^{2+} ions in living cells, including those from cancer and blood samples.
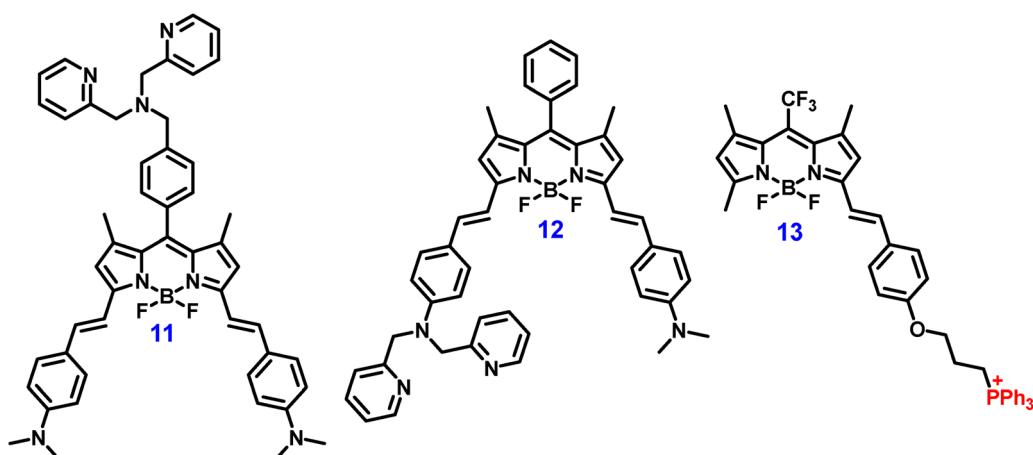

Fig. 13 Chemical structures of probes **11–13**. (Redrawn the ChemDraw structures from ref. 81–83).

12844 | *J. Mater. Chem. B*, 2025, **13**, 12831–12868

This journal is © The Royal Society of Chemistry 2025
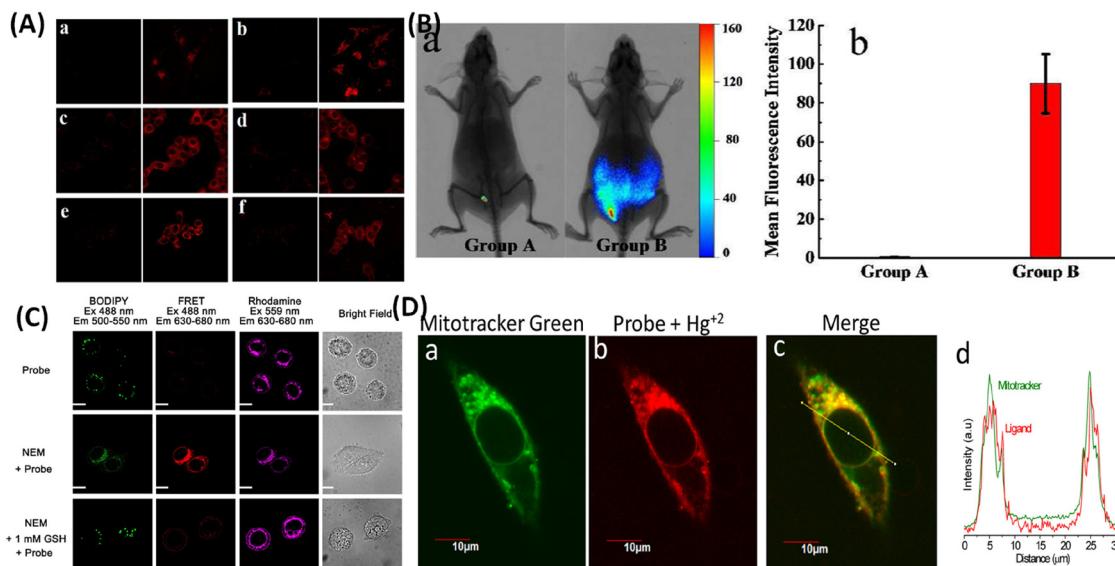
Fig. 14 (A) Fluorescence imaging of various cell lines (a)–(f) using probe **8** for H$_2$S$_n$ detection; the left side represents control cells, while the right side shows cells treated with both probe **8** and Na$_2$S$_2$. (B) *In vivo* fluorescence images of mice models: Group A treated with probe **8** alone, and Group B with both probe **8** and Na$_2$S$_2$; corresponding quantitative analysis included. Reproduced with permission from ref. 78, Copyright 2015 American Chemical Society. (C) Confocal imaging of HeLa cells stained with FRET-based ratiometric probe **10** in the absence and presence of GSH, and with NEM (thiol-reactive reagent) treatment. Reproduced with permission from ref. 80, Copyright 2020 Elsevier. (D) Co-localization images of probe **12** with Hct116 cells for selective Hg^{2+} detection. Reproduced with permission from ref. 82, Copyright 2016 American Chemical Society.

Das *et al.* advanced this strategy with probe **12**, a styryl BODIPY derivative containing a dipicolylamine group for Hg^{2+} sensing (Fig. 13 and 14D).[82] The probe **12** initially exhibits a weak fluorescence due to ICT from the donor amine to the BODIPY acceptor, which narrows the energy gap between frontier orbitals. However, upon specific binding to Hg^{2+}, this ICT is suppressed, leading to a blue shift in absorption and a significant fluorescence enhancement with an emission peak at 650 nm upon 620 nm excitation. The probe **12** showed high selectivity for Hg^{2+} over other biologically relevant metal ions, with a detection limit (LOD) of 0.17 μM, low cytotoxicity, good cell membrane permeability, and was effective for detecting Hg^{2+} specifically within mitochondria in colon cancer cells (Hct116 cells).

2.5 Chemical routes to far-red/NIR Mitochondria microenvironment probes: viscosity

Although numerous viscosity-sensitive fluorescent molecular rotors have been reported in the literature, several challenges remain that need urgent attention. These include a lack of NIR emissive molecular rotors, limited sensitivity, non-specific organelle targeting, and high background noise. To address these issues, Yan *et al.* developed a novel monostyryl BODIPY-based probe **13** having a trifluoromethyl (CF$_3$) group at the *meso*-position as a rotatable unit and a TPP$^+$ moiety for targeted mitochondrial imaging (Fig. 13, 15 and 16).[83] This probe exhibited a red shift in both absorption and emission (by 70 nm) compared to conventional mono-styryl BODIPY derivatives, though with reduced fluorescence due to the dynamic rotation of the CF$_3$ group. The free rotation of this *meso*-CF$_3$ group effectively quenched fluorescence in low-viscosity environments like water. However, in high-viscosity conditions (*e.g.*, glycerol), fluorescence intensity at
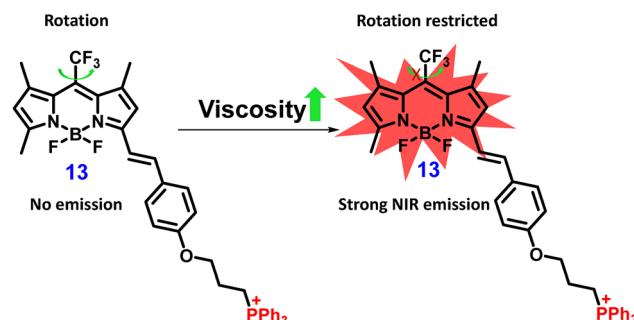

Fig. 15 Sensing mechanism of probe **13**. (Redrawn the ChemDraw structures from ref. 83).

657 nm increased significantly, with a detection limit of 0.48 cP. Probe **13** was insensitive to environmental parameters such as solvent polarity and competing species, and showed low cytotoxicity. Further, mitochondrial intracellular viscosity detection was confirmed using lipopolysaccharide (LPS) and nystatin treatments in SH-SY5Y cells, which caused a rise in intracellular viscosity and resulted in a 38-fold increase in red fluorescence. Relative to earlier mitochondrial probes for reactive species or ions, probe **13** shows how molecular rotor-based designs enable direct mapping of mitochondrial microenvironments, providing complementary information beyond chemical reactivity.

2.6 Chemical routes to far-red/NIR mitochondrial photosensitizers: PDT

PDT is an innovative and clinically approved therapeutic technique that harnesses the photodynamic effect. It has recently

This journal is © The Royal Society of Chemistry 2025

J. Mater. Chem. B, 2025, **13**, 12831–12868 | **12845**
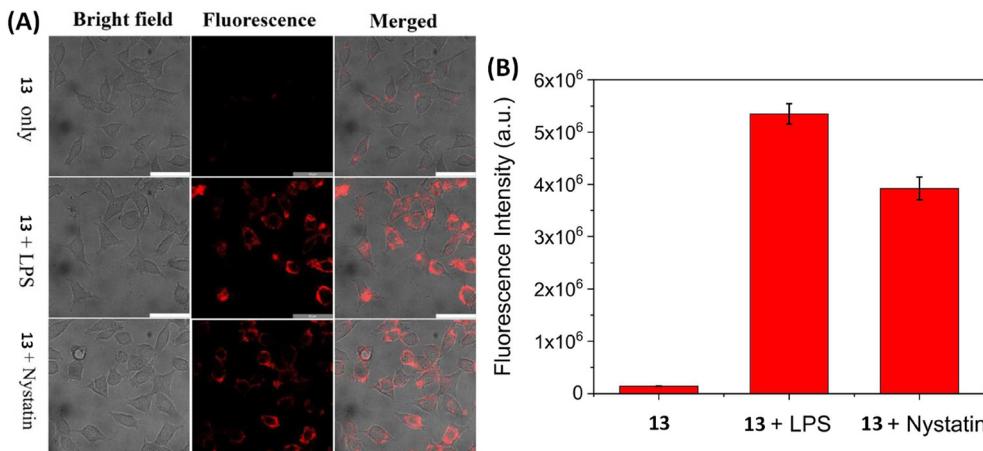
Fig. 16 (A) Confocal images of SH–SY5Y cells incubated with probe **13** (5 μM) only for 30 min; the cells were pretreated with LPS and nystatin (20 μM) for 40 min and then treated with probe **13** (5 μM) for another 30 min. (B) Fluorescence intensity plot of probe **13** pretreated with none, LPS, and nystatin. (λ_{ex} = 633 nm, λ_{em} = 650–750 nm). Reproduced with permission from ref. 83, Copyright 2022 Elsevier.

emerged as a research hotspot for treating diseases like cancer, owing to its non-invasiveness, minimal photodamage to surrounding healthy tissues, absence of drug resistance even after repeated use, and effectiveness in targeting both malignant and benign tumors. PDT comprises three key components: a photosensitizer, light with a specific wavelength, and molecular oxygen for the generation of ROS, especially singlet oxygen ($^1O_2$) to kill cancer cells. Upon light irradiation, the photosensitizer at the targeted site undergoes excitation from the singlet ground state (S_0) to the short-lived singlet excited state (S_n). It can then either relax back to the ground state by emitting fluorescence (radiative decay) or undergo intersystem crossing (ISC) to a more stable and longer-lived triplet excited state (T_1). In the triplet state, the photosensitizer can initiate photochemical reactions via two pathways: (a) involves hydrogen atom abstraction or electron transfer to form free radicals, which subsequently react with molecular oxygen to generate ROS (Type I reaction), (b) involves direct energy transfer from the excited photosensitizer to ground-state molecular oxygen ($^3O_2$), producing singlet oxygen ($^1O_2$) (Type II reaction), which causes oxidative damage leading to cancer cell death. Recent research highlights mitochondria as a promising target for PDT due to their distinct characteristics in cancer cells. These include elevated ROS production due to mitochondrial dysfunction and a more negatively charged mitochondrial membrane potential, which enhances the selective binding and retention of photosensitizers. However, many existing photosensitizers face challenges such as non-specific binding, low water solubility, limited cellular uptake, and off-target toxicity.

To address these limitations, Yan and co-workers reported probe **14**, a mitochondria-targeted NIR BODIPY-based photosensitizer (Fig. 17).[84] The design incorporated two triethylene glycol (TEG) chains at the 3,5-positions of the BODIPY core via Knoevenagel condensation with benzaldehyde, which simultaneously extended conjugation for NIR absorption/emission and enhanced hydrophilicity of the probes. To further boost performance, particularly to maximize the spin–orbit coupling

(SOC) and ISC processes, bromine atoms were introduced at the lateral 2 and 6 positions of the BODIPY core, and a quaternary ammonium group was added at the *meso* position to maintain hydrophilic balance and serve as a mitochondrial targeting moiety. The probe **14** exhibited a singlet oxygen quantum yield (ϕ_A) of 4.5%, minimal dark cytotoxicity, and high phototoxicity (IC$_{50}$ of HeLa = 46.93 nM, IC$_{50}$ of MCF-7 = 22.84 nM), and mitochondria-specific imaging. Although the fluorescence quantum yields in aqueous environments were relatively low, interactions with cellular components may stabilize the dye structure by increasing its rigidity, which in turn reduces non-radiative decay and enhances its efficiency as a mitochondria-specific photosensitizer via apoptosis of cancer cells. Together, these advances highlight that by carefully tuning substituents (e.g., electron-withdrawing groups, heavy atoms, or ionic targeting units), BODIPY derivatives can be tailored for monitoring mitochondrial microenvironments, detecting bioactive species, or enabling phototherapeutic applications.

2.7 Challenges and future perspectives of mitochondrial-targeting probes

Mitochondria-specific NIR probes are powerful tools for monitoring the intrinsic dynamic cellular processes, activities of bioactive species, and for disease treatments. Although numerous probes are synthesized for mitochondrial targeting, they suffer from some inherent drawbacks, such as:

(1) Cationic lipophilic probes often suffer from leakage from the matrix and can be washed out due to changes in the MMP during cellular stress, mitophagy, or drug treatments, which results in inaccurate detection signals and non-specific binding. Recently, mitochondria-immobilizable probes have gained attention since they can bind tightly, specifically, and selectively to mitochondria for the detection of bioactive species and microenvironment. For example, the aldehyde group can covalently bind to the amino groups of proteins to immobilize the probe

(2) Further, genetically encoded probes can also be utilized for covalent binding to mitochondria; however, gene transfection

12846 | *J. Mater. Chem. B*, 2025, **13**, 12831–12868

This journal is © The Royal Society of Chemistry 2025
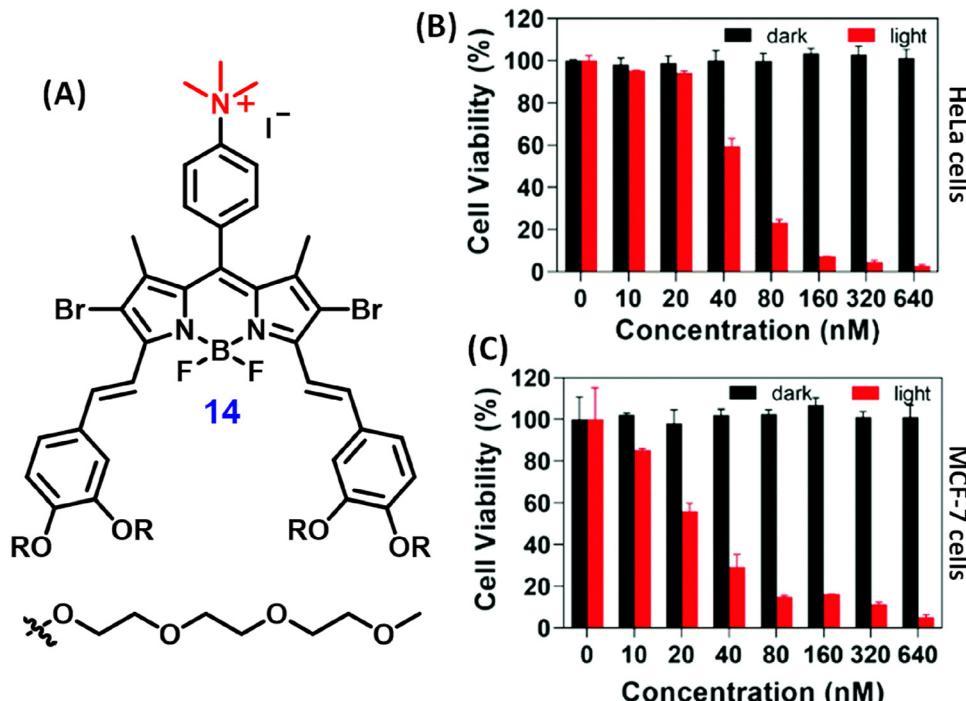
Fig. 17 (A) Chemical structure of probe **14** (Redrawn the ChemDraw structure from ref. 84). Dose–dependent cell proliferation (MTS) assay data conducted on probe **14** using HeLa cells (B) and MCF-7 cells (C) without and with LED light irradiation at 690 nm for 30 min. Data represent mean values, and error bars denote standard deviation (*n* = 3). Reproduced with permission from ref. 84, Copyright 2022 Royal Society of Chemistry.

efficiency varies after repeated washing due to changes in the micro-environmental parameters, which is not desirable for *in vivo* imaging

(3) In terms of long-time monitoring, cellular cytotoxicity is still a critical challenge

(4) Since mitochondria contain hundreds of biomolecules such as DNA, RNA, enzymes, proteins, lipids, cations, anions, *etc.*, selective targeting of a specific species at ultralow concentrations is rare and needs further innovations

(5) Instead of single emission probes, which are prone to photobleaching and other environmental interferences, the self-calibrating feature of ratiometric probes (utilizes the ratio of two fluorescent signals) makes it a promising tool for quantitative measurement of analytes, biosensing, and imaging applications with enhanced accuracy and reliability

3. Lysosomal localized probes

3.1 Overview of lysosomal dynamics

Lysosomes are acidic, membrane-bound organelles found in most eukaryotic cells, typically ranging in shape from spherical to elliptical (0.2–0.8 μm diameter), serving as the primary catabolic and recycling centre.[85] Often called "suicide bags," they contain >60 hydrolytic enzymes, including proteases, lipases, glycosidases, nucleases, acid phosphatases, and sulfatases that break down endogenous and exogenous biomacromolecules *via* autophagy, endocytosis, and phagocytosis.[86] Their acidic environment (pH 4.5–5), essential for enzymatic activity, is regulated by lysosomal membrane proteins such as

vascular ATPase (v-ATPase) through ATP-driven proton pumping between the cytoplasm and lysosome, ensuring high membrane stability and selective permeability.[86,87] Additionally, heavily glycosylated proteins like LAMP-1 and LAMP-2 safeguard the membrane from self-degradation and provide structural integrity.[87] They are dynamic organelles playing significant roles in signal transduction, immune defense, organelle cross-talk *via* fission and fusion, and cellular metabolism (growth, division, aging, death).[10,86] Lysosomal homeostasis of complex internal microenvironment (pH, polarity, viscosity, ion balance (Ca^{2+}, H^+, Na^+, K^+, Zn^{2+})) and biological species (RONSS) is vital for normal physiological processes, and any dysfunction/dysregulation can result in diseases such as lysosomal storage disorders (LSDs), neurodegenerative diseases, and cancer.[87,88] For example, in order to meet the metabolic demands for proliferation and growth, cancer cells upregulate the lysosomal activities (number, distribution, autophagy, biological species, *etc.*).[10] Consequently, real-time monitoring of lysosomal functions and dysfunctions opens a new therapeutic window for early disease diagnosis and precision medicine.[89–91] Hence, it underscores the pressing need to generate new fluorescent probes that can specifically target lysosomes with enhanced biocompatibility, selectivity, sensitivity, stability, and performance.

3.2 General design rules for lysosomal probes

The development of effective lysosomal probes requires precise chemical engineering to ensure organelle specificity, environmental responsiveness, minimal cytotoxicity and photostability. Some key design strategies include:

This journal is © The Royal Society of Chemistry 2025

J. Mater. Chem. B, 2025, **13**, 12831–12868 | **12847**

(1) Environment-sensitive functionalization: probes are often functionalized with lipophilic amine groups (e.g., morpholine or N,N-dimethylamine derivatives) that respond to the acidic pH of lysosomes. Upon protonation in the lysosomal lumen, these groups become positively charged, leading to probe retention via pH-dependent membrane trapping and reduced permeability, enabling precise lysosomal localization.[85,88,89]

(2) Endocytosis-driven targeting via nanoaggregates: another strategy involves engineering surface-modified probes with hydrophilic polymers that enable endocytotic uptake. The quenched nanoaggregates in the blood get activated (disaggregation) upon endocytosis to lysosomes due to non-covalent interaction and acidic nature, thereby eliminating background fluorescence and enhancing sensitivity and contrast.[85,92]

(3) Targeting lysosomal biomolecules and enzymes: probes can also be tailored to interact selectively with lysosomal components such as hydrolytic enzymes, membrane proteins, or bioactive molecules, including ROS, RNS, and RSS. These interactions enable the probes to sense and report specific biochemical events and changes within the lysosomal environment.[16,88–90]

3.3 Chemical routes to far-red/NIR lysosomal microenvironment probes and their biomedical applicability

A summary of the photophysical properties of lysosomal NIR BODIPY probes is given in Table 2.

3.3.1 pH responsive probes. Given the acidic pH of lysosomes, a common targeting strategy involves functionalizing BODIPY fluorophores with lipophilic amine groups. In this context, Zeng et al. engineered a morpholine-substituted BODIPY probe **15** incorporating electron-donating di-indolyl styryl derivatives at the 3,5-positions (Fig. 18).[93] This structural modification extended the π-conjugation and shifted the absorption and emission maxima into the NIR region (λ_{ab} = 680 nm, λ_{em} = 727 nm in ethanol). The lower flexibility of styryl substitutions resulted in low quantum yield (ϕ_F = 0.09). Further, the probe **15** demonstrated remarkable stability and enhanced emission profile across the acidic pH range (2.5–5), while non-emissive in alkaline environments due to deprotonation of its phenolic hydroxyl groups. Moreover, it showed excellent biocompatibility, strong resistance to photobleaching, minimal cytotoxicity, and high selectivity for lysosomes in HeLa cells, without interference from other biologically relevant species. Co-localization experiments demonstrated strong lysosomal specificity of the probe, with a Pearson correlation coefficient of 0.81 when compared to LysoTracker Red DND-99. Moreover, the probe exhibited excellent photostability, with less than 8.7% reduction in fluorescence intensity after 30 minutes of continuous laser exposure in HeLa cells, highlighting its strong resistance to photobleaching, a key requirement for reliable bioimaging applications.

To improve hydrophilicity and cellular uptake, O'Shea and colleagues developed a PEGylated, lysosome-targeted pH-sensitive NIR probe **16** for real-time monitoring of dynamic cellular processes such as endocytosis, trafficking, and efflux (Fig. 18, 19 and 20A).[94] This system utilized an ortho-nitrophenol moiety that quenches fluorescence via ICT at neutral pH but restores emission in acidic lysosomal conditions through protonation. The probe showed excellent photostability and is unaffected by polarity changes, making it well-suited for long-term imaging. It remains non-fluorescent under neutral conditions but is selectively activated in acidic lysosomes, resulting in high signal-to-noise with minimal background fluorescence. This pH-responsiveness enables detailed 3D/4D live-cell imaging of lysosomal processes such as endocytosis and trafficking, as demonstrated in LAMP1-GFP (lysosomal-associated membrane protein 1-green fluorescent protein) HeLa cells. The probe also showed strong potential for in vivo tumor imaging, clearly distinguishing tumor regions, making it a valuable tool for tracking lysosomal processes and targeted bioimaging.

Meanwhile, Liu et al. synthesized a piperazine-functionalized di-styryl BODIPY probe **17** to monitor lysosomal pH via modulations in both ICT and PET (Fig. 18 and 20B).[95] Under neutral or basic pH, the strong ICT from the donor piperazine to the acceptor BODIPY core, and PET from the lower nitrogen atom of piperazine to the BODIPY, quenched the fluorescence, whereas at acidic pH, protonation of piperazine groups inhibited these quenching mechanisms, resulting in strong emission. To enhance aqueous solubility, oligo(ethylene glycol) chains were introduced at multiple sites. The probe **17** displayed NIR absorption/emission (687/750 nm), a broad dynamic pH detection range (pH 7.4–4.2), excellent photostability, and selective pH responsiveness. Despite lower cellular uptake (3%) and weak fluorescence (possibly due to increased steric hindrance and hydrophilicity), the system showed strong sensitivity to intracellular pH variations and negligible cytotoxicity in both cancerous (MDA-MB-231) and normal (HUVEC-C) cell lines. Together, these studies illustrate distinct design strategies for engineering pH-responsive lysosomal probes, establishing BODIPY scaffolds as versatile platforms for lysosomal pH imaging and tumor diagnostics.

3.3.2 Polarity responsive probes. Beyond acidity, lysosomal polarity is another vital microenvironmental factor that regulates cellular physiology and protein interactions, serving as a key indicator of metabolic disorders and disease progression. To address this, Feng et al. developed a polarity-sensitive lysosomal-targeted NIR probe **18** for the detection of lung and liver damage associated with diabetes (Fig. 21).[96] The design strategy comprises two primary approaches: (1) Knoevenagel condensation of 4-(4-methylpiperazine)benzaldehyde with BODIPY at the 3,5 positions for extended conjugation and NIR absorption (λ_{ab} = 700 nm) and emission (λ_{em} = 758–812 nm), and (2) a pH-sensitive methyl piperazine moiety to ensure lysosomal targeting via protonation. Probe **18** exhibited selectivity to polarity, was insensitive to viscosity variation, and remained stable within the lysosomal pH range (4.0–5.5). Additionally, studies using hyperglycaemic-stimulated models in A549 and HepG2 cells indicated that elevated glucose concentrations (50 mM) may reduce lysosomal polarity, resulting in increased fluorescence with extended stimulation duration. Importantly, in diabetic mouse models, the probe enabled simultaneous imaging of lung and liver damage, with the lungs showing a more pronounced fluorescence enhancement, highlighting the probe's diagnostic value for diabetes-associated complications.

12848 | J. Mater. Chem. B, 2025, **13**, 12831–12868

This journal is © The Royal Society of Chemistry 2025

Journal of Materials Chemistry B

Table 2   Summary of photophysical properties of Lysosomal NIR BODIPY probes
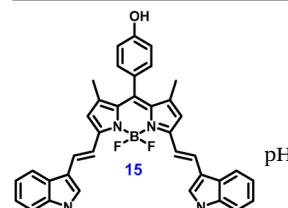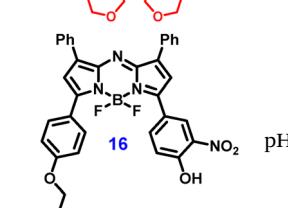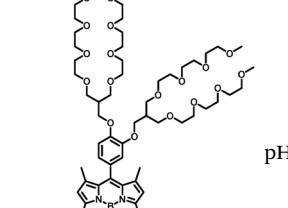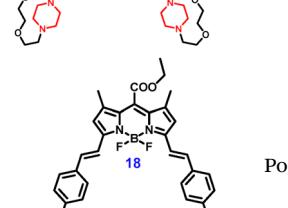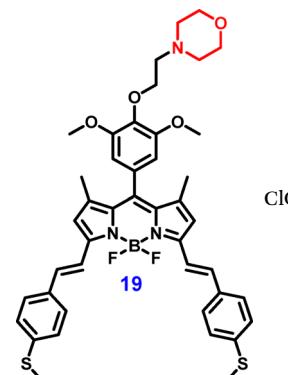
| Probes (P)	Analytes	Solvent	$\lambda_{ex}/\lambda_{em}$ (nm)	QY (ϕ_F)	Probe Conc/ dynamic range (μM)	LOD	Comments	Ref.
15	pH	Ethanol	680/727	0.09	—	—	Morpholine probe for lysosomal labeling	93
16	pH	DMEM (10% FBS) pH 2	685/707	0.18	—	—	Real time imaging of lysosomal processes such as endocytosis, trafficking and efflux in 3D and 4D, *in vivo* tumour imaging using an MDA-MB-231 tumour model	94
17	pH	Buffer pH 7.4	687/750	<0.01	—	—	pH responsive piperizine probe for *in vitro* lysosome imaging inside normal endothelial and breast cancer cells	95
18	Polarity	Toluene and MeOH	709/756 and 695/774	0.499 and 0.068	—	—	Polarity sensitive piperazine probe for *in vivo* imaging of injured lung and liver in diabetes mice model	96
19	ClO$^-$	DMF/PBS (4/6, pH 7.4)	650, 630/685, 650	P: 0.28 P. ClO$^-$: 0.32	10 μM/0–80 μM	45 nM	Lysosome targeting ratiometric probe; morpholine probe for ClO$^-$ detection in living cells, diabetic mice models	97

Table 2 (*continued*)
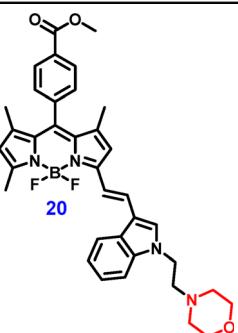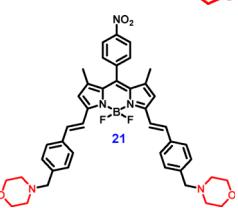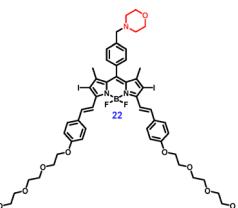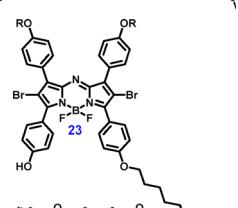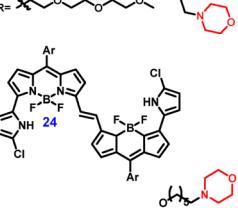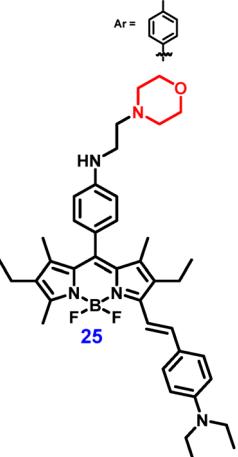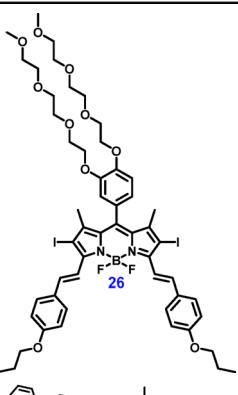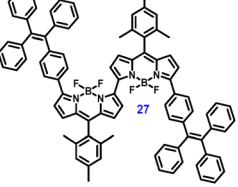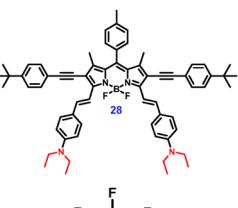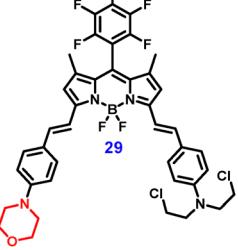
Probes (P)	Analytes	Solvent	$\lambda_{ex}/\lambda_{em}$ (nm)	QY (ϕ_F)	Probe Conc/ dynamic range (μM)	LOD	Comments	Ref.
20	Carboxylesterase1 (CES1)	PBS/CH₃CN	595/638	0.53	10 μM/0– 10 μg mL⁻¹	2.15 μg mL⁻¹	Morpholine probe for detection of carbamates pesticide (carbaryl) as well as CES1 in lysosome of HepG2 cells	98
21	—	DCM	638/647	0.06	—	—	Lysosome targeting morpholine probe for imaging hypoxic cells	99
22	—	DCM	660/694	0.11	—	—	$^1O_2$ mediated PDT; lysosomal imaging IC$_{50}$ (light): 0.2 mM (MCF-7)	100
23	—	PBS (pH 7.4)	685/710	0.02	—	—	$^1O_2$ mediated PDT *via* apoptosis; lysosomal imaging IC$_{50}$ (light): 0.48 μM (HeLa)	101
24	—	Toluene	846/983	0.02	—	—	PTT agent; lysosomal imaging IC$_{50}$ (light): 9.4 μM (HeLa)	102
25	—	PB	632/770	0.10	—	—	Combined therapy: PDT and PTT agent; lysosomal imaging IC$_{50}$ (light): 15.7 μM (HeLa), 11.6 μM (4T1)	103

12850 | *J. Mater. Chem. B*, 2025, **13**, 12831–12868

This journal is © The Royal Society of Chemistry 2025

Table 2 (continued)

Probes (P)	Analytes	Solvent	$\lambda_{\text{ex}}/\lambda_{\text{em}}$ (nm)	QY (ϕ_F)	Probe Conc/ dynamic range (μM)	LOD	Comments	Ref.
26	—	20% drug loaded (20% micelles)	730/785	< 0.01	—	—	Combined therapy: PDT and PTT agent; lysosomal imaging IC$_{50}$ (light): 16.2 μg mL^{-1} (4T1)	104
27	—	DCM	742/810	0.11	—	—	Combined therapy: PDT and PTT agent; lysosomal imaging IC$_{50}$ (light): 4.1 μM (HeLa)	105
28	—	DMF	760/830	—	—	—	Combined therapy: PDT and PAI agent; lysosomal imaging	106
29	—	PBS	731/820	0.103 (ethanol)	—	—	Multimodal therapy therapy: PDT, PTT and chemotherapy agent; lysosomal imaging; IC$_{50}$ (light): 8.75 μM (HeLa), 10.02 μM (4T1)	107

3.4 Chemical routes to far-red/NIR lysosomal biosensing probes and their biomedical applicability

Lysosomal homeostasis relies not only on acidic pH and polarity but also on adaptation to other microenvironmental factors such as reactive species and enzymatic activity, which are crucial for sustaining redox balance and energy metabolism. Dysregulation of these parameters is closely associated with lysosomal dysfunction and disease progression, thereby underscoring the demand for advanced fluorescent probes capable of precise monitoring within the lysosomal microenvironment.

3.4.1 Detection of hypochlorous acid (HClO). Wang *et al.* reported a novel lysosome-targeted, BODIPY-based NIR ratiometric fluorescent probe **19** capable of detecting both exogenous and endogenous HClO in living cells, zebrafish, and diabetic mouse models (Fig. 22, 23 and 25A).[97] The probe design integrates three key components: a BODIPY core as the fluorophore,

a morpholine moiety for lysosome-specific localization, and a thioanisole group serving as the HClO recognition site. The sensing mechanism is based on the inhibition of ICT from thioanisole (donor) to BODIPY (acceptor): in the presence of HClO, the thioether group is selectively oxidized to sulfoxide, disrupting ICT and triggering a ratiometric shift in the NIR fluorescence spectrum. Specifically, with increasing HClO concentrations (0–80 μM), the absorption and emission maxima at 650 nm and 685 nm, respectively, diminished and blue-shifted to 630 nm and 650 nm. Notably, the probe also functions as a colorimetric sensor, visibly shifting from blue to green under ambient light. Probe **19** demonstrated a fast response time (< 20 s), low detection limit (LOD = 45 nM), high quantum yield, strong ratiometric emission, excellent selectivity for HClO over competing species, low cytotoxicity, and high biocompatibility. In cellular models (RAW264.7 and HepG2), the probe enabled real-time

This journal is © The Royal Society of Chemistry 2025

J. Mater. Chem. B, 2025, **13**, 12831–12868 | **12851**
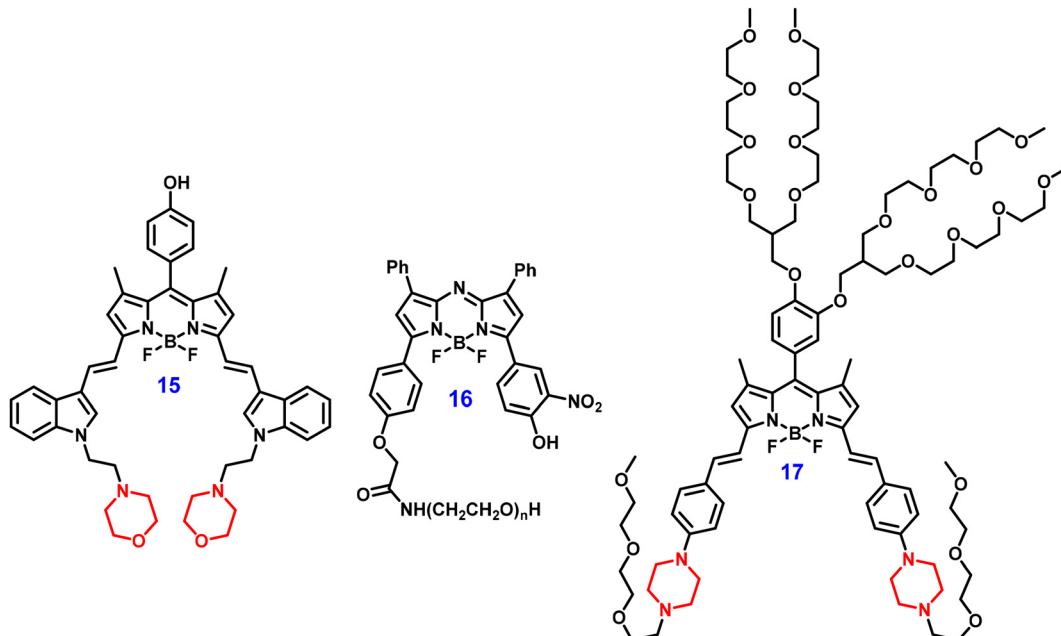
Fig. 18 Chemical structures of compounds **15–17**. (Redrawn the ChemDraw structures from ref. 93–95).
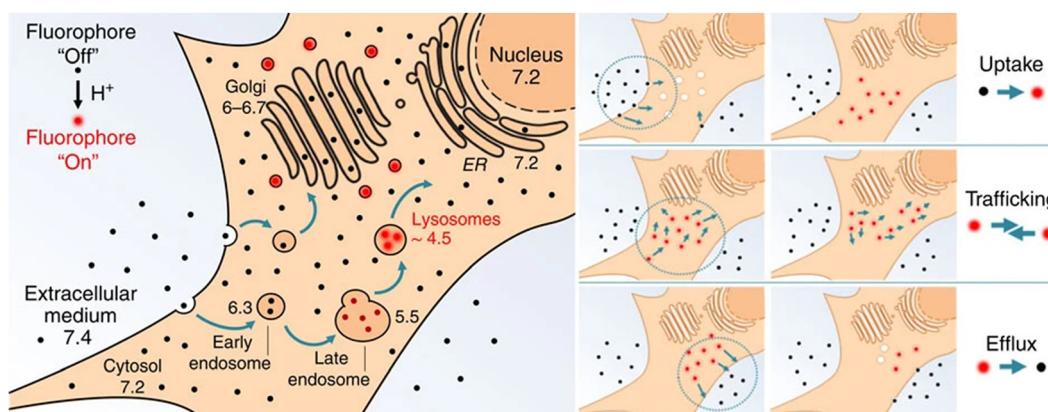

Fig. 19 Proposed cellular uptake mechanism and the three observable stages (uptake, trafficking, and efflux) of the path of probe **16** in the cellular environment. Reproduced with permission from ref. 94.

monitoring of HClO dynamics, and *in vivo* studies in diabetic mice revealed its potential for assessing HClO-induced damage in the liver and kidneys, the primary HClO-targeted organs. These attributes position the probe as a promising tool for early diagnosis and therapeutic evaluation of diabetes.

3.4.2 Monitoring carboxylesterase 1 (CES1) activity and pesticide exposure. Carboxylesterases (CES) are serine hydrolases that catalyze the hydrolysis of diverse substrates, including esters, amides, thioesters, lipids, and carbamates. CES play a central role in the detoxification of pesticides, environmental toxins, and in drug metabolism, functioning both as drug targets and as activators of prodrugs through irreversible interactions at their active sites. Abnormal CES expression has been implicated in various diseases, including atherosclerosis, obesity, type 2 diabetes mellitus, and liver cancer. Consequently, the development of specific fluorescent probes for monitoring CES1 levels

and activity in biological systems is of significant importance. Considering this, Huang *et al.* developed a NIR-emissive, lysosome-targeted BODIPY probe **20** for monitoring the activity of CES1, both under physiological conditions and following pesticide exposure (Fig. 22, 24, and 25B).[98] The design incorporated a morpholine group for lysosomal localization, a methyl formate ester at the *meso*-position as the CES1 recognition site, and an electron-donating indole-3-carboxaldehyde group for NIR emission (λ_{ab} = 595 nm, λ_{em} = 638 nm). The sensing mechanism involves CES1-mediated hydrolysis of the methyl formate group (ester bond), to an electron-withdrawing carboxyl group that diminishes fluorescence intensity. The probe **20** exhibited high CES1 selectivity, excellent stability across a wide pH range (3–10), and low cytotoxicity, with lysosomal specificity in HepG2 cells. Moreover, it proved effective for evaluating the impact of carbaryl (quantitative detection), a carbamate pesticide, on CES1 activity.

12852 | *J. Mater. Chem. B*, 2025, **13**, 12831–12868

This journal is © The Royal Society of Chemistry 2025
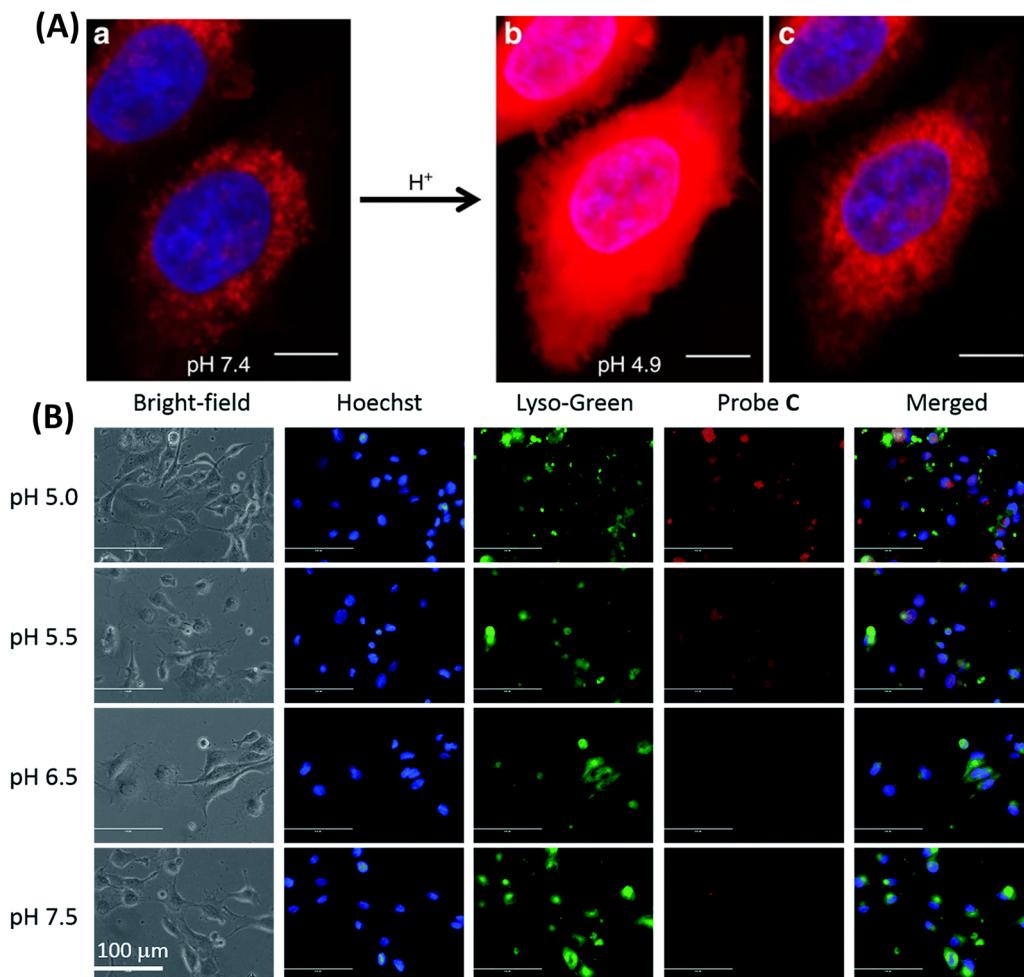
Fig. 20 (A) Confocal fluorescence images of HeLa cells incubated with probe **16** at varying pH values, demonstrating pH-responsive behavior. Reproduced with permission from ref. 94. (B) Fluorescence images of HUVEC-C cells treated with probe **17** under different pH conditions, highlighting its pH sensitivity. Reproduced with permission from ref. 95, Copyright 2015 Royal Society of Chemistry.

Carbaryl binds irreversibly to CES1's active site, inhibiting its function and altering the fluorescence response. This probe thus offers a novel approach for assessing pesticide-induced enzymatic inhibition at the subcellular level, providing a foundation for next-generation pesticide detection tools.

3.4.3 Hypoxia-responsive lysosomal imaging. In contrast to probes **19** and **20**, which respond to specific reactive or enzymatic stimuli, Lu *et al.* addressed lysosomal microenvironmental stress by synthesizing a bis-styryl BODIPY probe **21** functionalized with morpholine groups at the 3,5-positions for lysosomal targeting and a *p*-nitrophenyl substituent at the *meso*-position for hypoxia sensing (Fig. 26).[99] The electron-withdrawing nitro group facilitates oxidative PET, leading to quenched fluorescence, which can be restored upon reduction of the nitro group under hypoxic conditions. This "turn-on" response allowed the probe to selectively visualize hypoxic conditions in HepG2 cells, with significantly enhanced emission observed under 1% O_2. Co-localization studies with LysoTracker Green demonstrated that the probe achieved approximately 96% lysosomal specificity. In addition, it outperformed the commercial MB in terms of photostability and biocompatibility, making it a superior candidate for NIR

lysosome-targeted fluorescence imaging in live cells. Notably, lysosomal specificity and hypoxia sensitivity make the probe a valuable candidate for imaging tumor microenvironments and guiding hypoxia-targeted therapies.

3.5 Chemical routes to far-red/NIR lysosomal photosensitizers

Apart from mitochondria, lysosomes are vital subcellular organelles and have emerged as promising therapeutic targets. As the primary digestive compartments of cells, they are responsible for the macromolecular degradation *via* endocytosis, phagocytosis, and autophagy. They also regulate cellular processes such as cell adhesion, migration, apoptosis, and overall homeostasis. Particularly, cancer cells often exhibit an increased number and volume of lysosomes to sustain homeostasis and adapt to stressful microenvironmental conditions. Moreover, lysosomal spatial distribution has been closely linked to cancer cell proliferation, invasion, metastasis, and energy metabolism. Unlike mitochondria, the absence of crucial antioxidant enzymes in lysosomes renders them more susceptible to oxidative stress and ROS-induced damage. Excessive oxidative stress

This journal is © The Royal Society of Chemistry 2025

*J. Mater. Chem. B*, 2025, **13**, 12831–12868 | **12853**
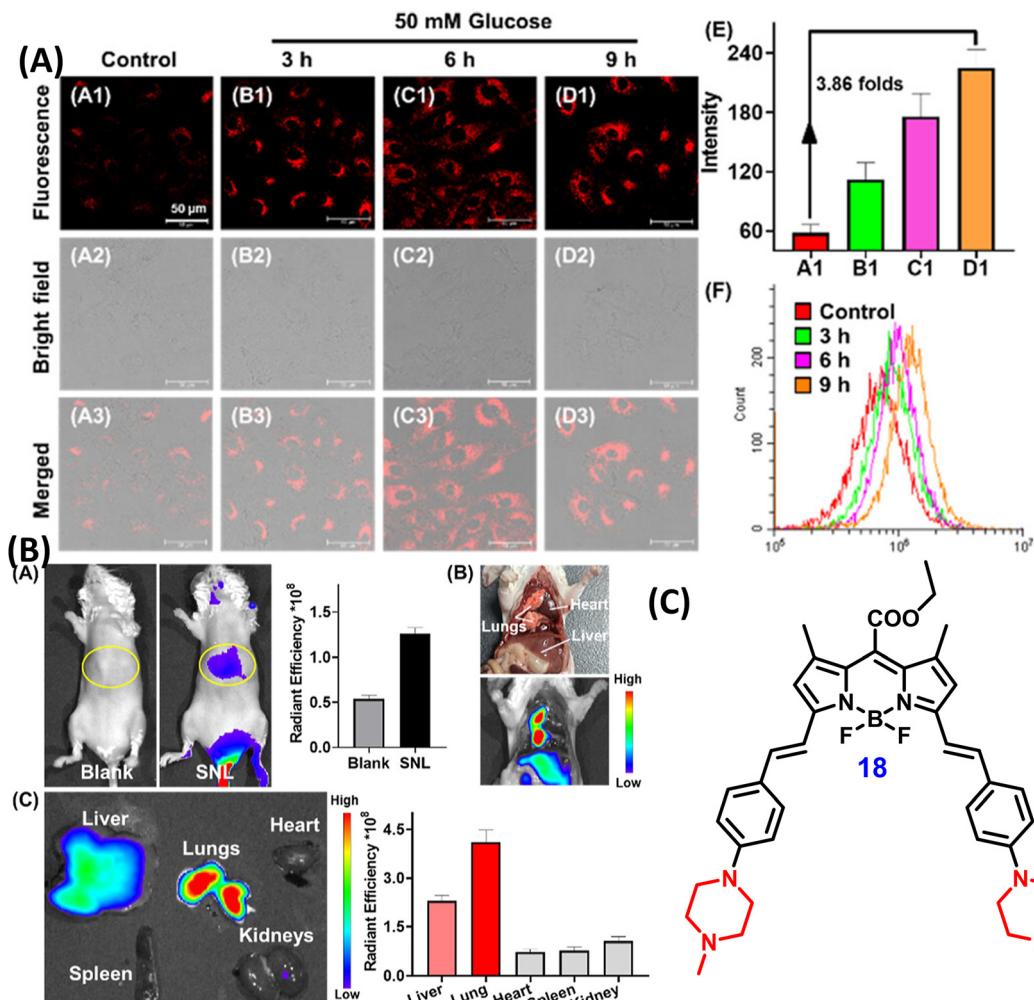
Fig. 21 (A) Confocal imaging, fluorescence intensity analysis, and flow cytometry of A549 cells treated with probe **18** under hyperglycemic conditions. (B) *In vivo* fluorescence imaging of probe **18** in a diabetic mouse model. (C) Chemical structure of probe **18**. Reproduced (A and B) with permission from ref. 96, Copyright 2024 American Chemical Society.

disrupts autophagic homeostasis, leading to cell death. However, lysosomal content leakage may also damage normal cells and induce side effects, emphasizing the need for further

Fig. 23 Proposed ratiometric detection mechanism of probe **19** to HClO. (Redrawn the ChemDraw structures from ref. 97).

research to elucidate ROS-mediated lysosomal dysfunction and optimize photosensitizer design for cancer therapy.

3.5.1 Photodynamic therapy (PDT). Recent developments in lysosome-targeted PDT (see Section 2.6 for a brief overview) have emphasized the design of NIR photosensitizers with improved singlet oxygen generation through the introduction


Fig. 22 Chemical structures of compounds **19** and **20**. (Redrawn the ChemDraw structures from ref. 97 and 98).

12854 | *J. Mater. Chem. B*, 2025, **13**, 12831–12868

This journal is © The Royal Society of Chemistry 2025
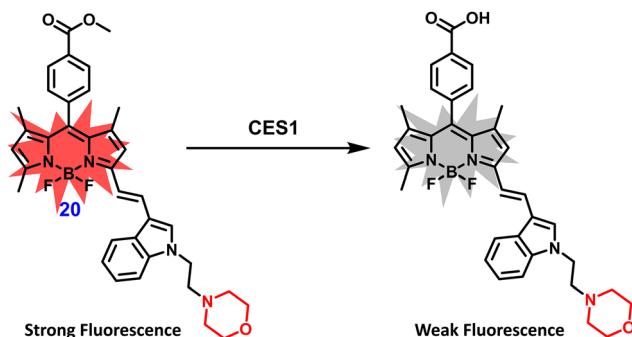
Fig. 24 Detection mechanism of probe **20** to CES1. (Redrawn the Chem-Draw structures from ref. 98).

of heavy atoms (*e.g.*, iodine), which enhance spin–orbit coupling and thereby facilitate the intersystem crossing (ISC) process. In parallel, structural modification with morpholine units has been employed to achieve subcellular specificity, as morpholine, a weakly basic amine with low ionic strength, preferentially accumulates in acidic lysosomes. For instance, Peng *et al.* designed a 2,6-diiodo BODIPY-based NIR photosensitizer (**22**) incorporating heavy iodine atoms to enhance intersystem crossing and singlet oxygen generation. To achieve lysosomal specificity, a morpholine moiety was introduced *via* nucleophilic substitution, while a PEG chain was attached through Knoevenagel condensation to improve aqueous solubility (Fig. 27). The probe **22** displayed strong NIR absorption (660 nm) and emission (694 nm), with a moderate fluorescence
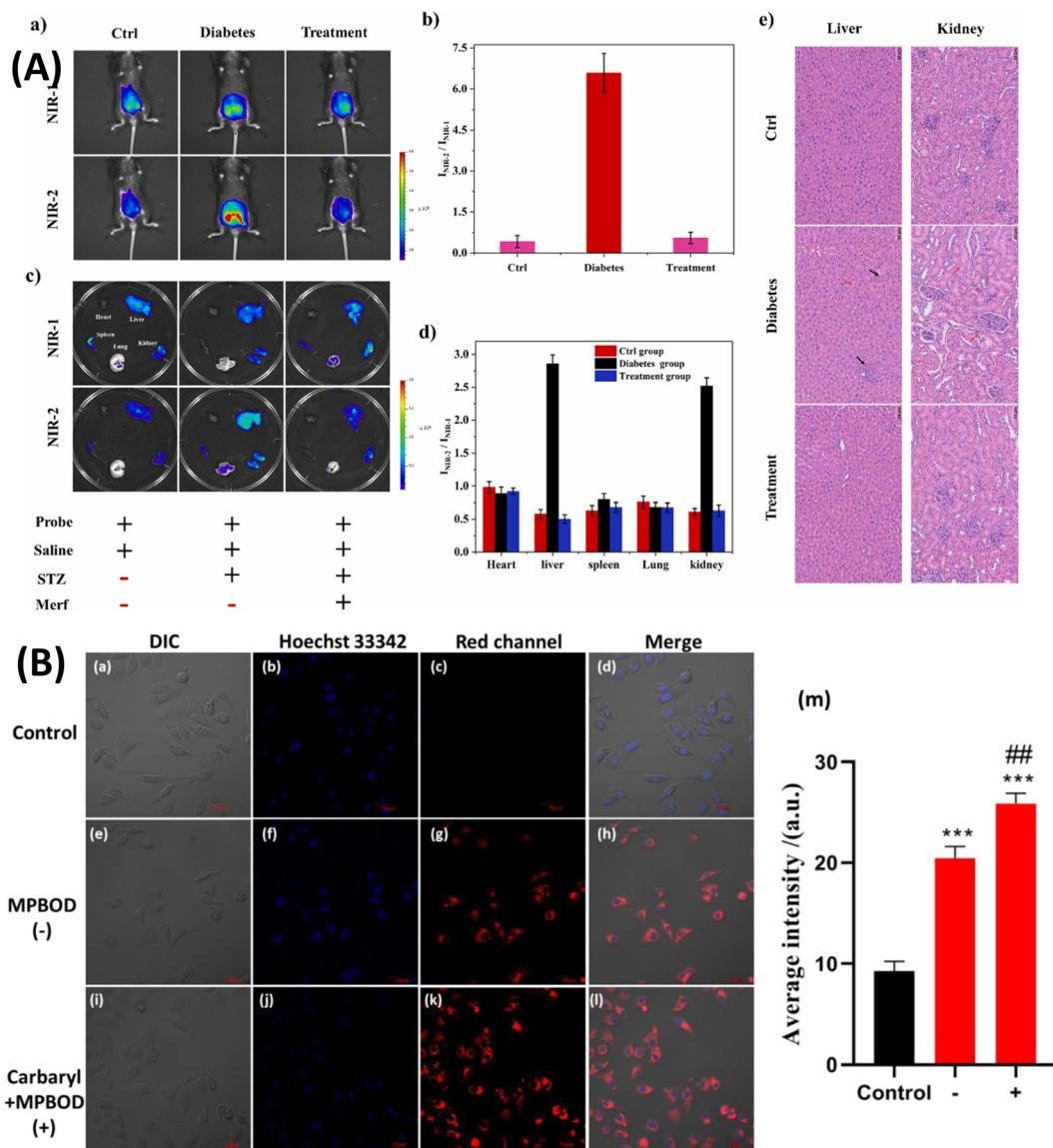
Fig. 25 (A) Confocal fluorescence imaging of diabetic mice models treated with probe **19** for visualizing endogenous HClO levels. Reproduced with permission from ref. 97, Copyright 2024 Elsevier. (B) Confocal fluorescence images of HepG2 cells stained with probe **20** under different conditions: control (probe alone), co-incubation with carboxylesterase 1 (CES1), and pre-treatment with the pesticide carbaryl followed by incubation with CES1 and the probe, illustrating CES1 activity detection and inhibition. Reproduced with permission from ref. 98, Copyright 2020 Elsevier.

This journal is © The Royal Society of Chemistry 2025

J. Mater. Chem. B, 2025, **13**, 12831–12868 | **12855**
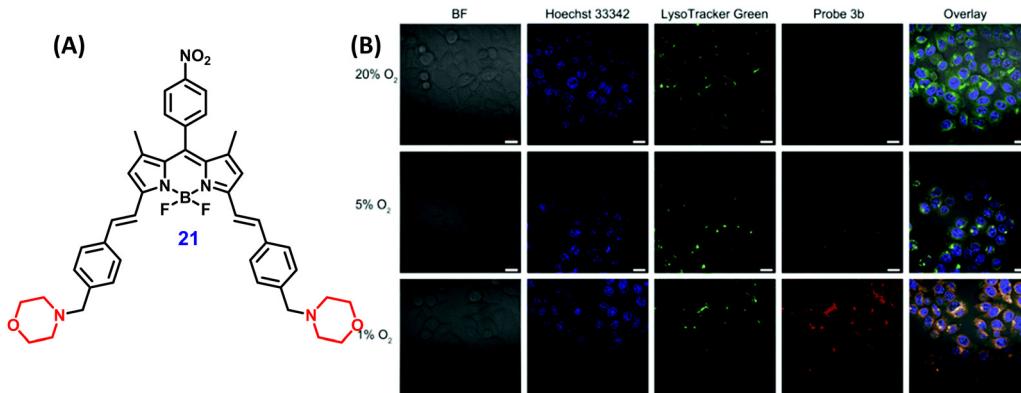
Fig. 26 (A) Chemical structure of probe **21**. (Redrawn the ChemDraw structures from ref. 99) (B) confocal images of HepG2 cells incubated with probe **21** under varying oxygen concentrations (hypoxic cells). Reproduced with permission from ref. 99, Copyright 2019 Royal Society of Chemistry.
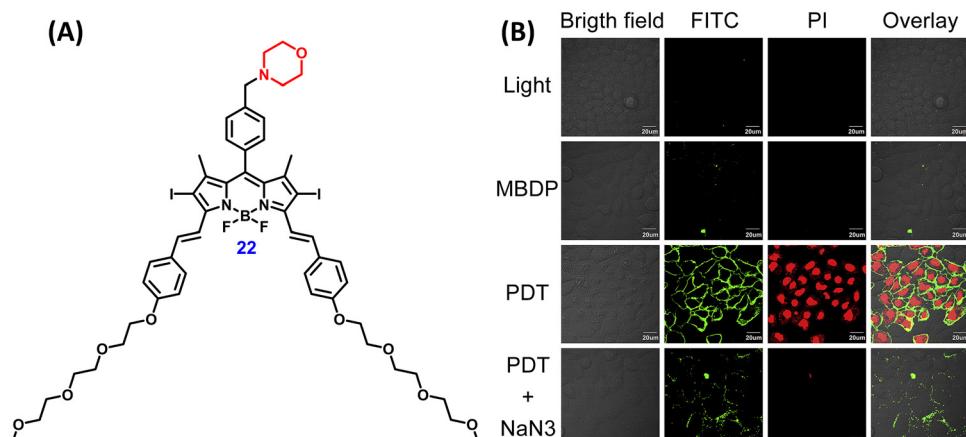
Fig. 27 (A) Chemical structure of probe **22**. (Redrawn the ChemDraw structures from ref. 100) (B) confocal fluorescence images of MCF-7 cells treated with probe **22** under various conditions: light irradiation, probe alone, and pre-treatment with $^1O_2$ scavenger NaN_3 demonstrating its PDT efficacy. Reproduced with permission from ref. 100, Copyright 2017 Elsevier.

quantum yield (ϕ_F = 0.11). Importantly, it demonstrated a superior singlet oxygen yield (ϕ_Δ = 0.64 in DCM) compared to MB (ϕ_Δ = 0.57), along with excellent photostability and low dark cytotoxicity. In MCF-7 cells, the photosensitizer exhibited high phototoxicity (IC_{50} = 0.2 mM), compared to the known photosensitizer Ce6 (IC_{50} = 1.39 mM), highlighting its efficacy in PDT-induced apoptosis.

Similarly, Lo *et al.* developed an aza-BODIPY photosensitizer (**23**) featuring dibromo substituents to promote intersystem crossing through the heavy atom effect and a morpholine group for lysosomal targeting (Fig. 28).[101] The precursor aza-BODIPY was prepared through a multistep synthesis, after which a six-carbon alkyl linker was introduced to minimize steric interference with the targeting unit. Final nucleophilic substitution with morpholine afforded the lysosome-selective probe **23**. Despite a low fluorescence yield (ϕ_F = 0.02), the probe **23** showed an excellent singlet oxygen yield (ϕ_Δ = 0.90 in DMF). The photosensitizer exhibited potent phototoxicity across multiple cancer cell lines, with an IC_{50} of 0.48 μM and IC_{90} of 0.95 μM in HeLa cells, confirming its robust ROS generation and lysosome-specific PDT activity through apoptosis.

3.5.2 Photothermal therapy (PTT). While probes **22** and **23** highlight lysosome-targeted BODIPY photosensitizers for PDT, complementary efforts have also explored photothermal therapy (PTT) using structurally engineered BODIPY derivatives to expand the therapeutic potential of these fluorophores. PTT is a promising cancer treatment strategy that converts light energy into localized heat using photothermal agents such as organic dyes. Its therapeutic precision can be controlled by modulating light intensity, exposure duration, and the concentration of photothermal materials, thereby minimizing damage to healthy tissues. PTT offers notable advantages, including high selectivity and specificity toward cancer cells; however, it is still limited by shallow tissue penetration, low photothermal conversion efficiency, and potential toxicity of the agents, which can compromise therapeutic outcomes. To overcome these challenges, Jiao *et al.* synthesized a π-extended BODIPY dimer (**24**) through a palladium-catalyzed Stille cross-coupling reaction between halogenated 3-pyrrolyl BODIPY and *trans*-1,2-bis(tributylstannyl)ethene, followed by nucleophilic substitution with morpholine at the *meso*-position (Fig. 28).[102] Interestingly, this reaction selectively activated the α-Cl atom on the BODIPY core, yielding a dimer with improved photothermal

12856 | *J. Mater. Chem. B*, 2025, **13**, 12831–12868

This journal is © The Royal Society of Chemistry 2025
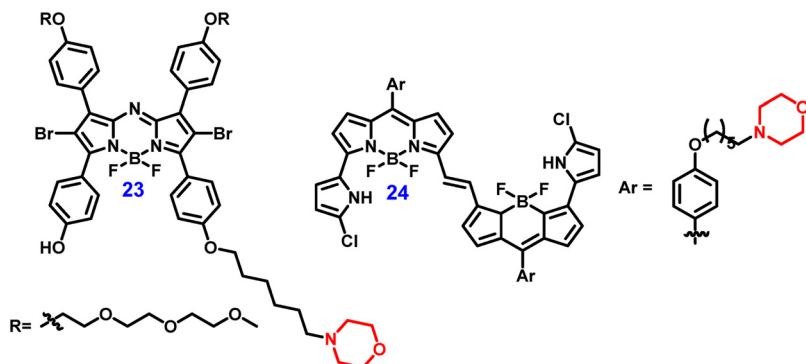
Fig. 28 Chemical structures of probes **23** and **24**. (Redrawn the ChemDraw structures from ref. 101 and 102).

properties. The probe **24** exhibited strong NIR absorption (λ_{ab} = 846 nm in toluene) and emission (λ_{em} = 983 nm), with a broad emission tail extending to 1200 nm. Although its fluorescence was weak (ϕ_F = 0.02), encapsulation within Pluronic F-127 significantly improved hydrophilicity and biocompatibility. Compared to ICG, the resulting nanoparticles (NPs) demonstrated superior photothermal performance: a high photothermal conversion efficiency (PCE) of 72.5%, elevated heating (66.7 °C under 808 nm laser), and strong optical and photothermal stability across multiple cycles. Furthermore, the probe displayed low dark cytotoxicity and potent phototoxicity (IC$_{50}$ = 9.4 µM) in HeLa cells, supporting its application as an effective NIR photothermal agent.

3.5.3 Combination therapies: PDT and PTT. Although PDT has gained considerable attention as a therapeutic modality, its clinical utility remains constrained by factors such as tumor size and location, limited targeting precision, and the oxygen dependence of most photosensitizers. Similarly, PTT faces challenges including shallow NIR light penetration, potential thermal injury to normal tissues, and the risk of local overheating. To address these limitations, synergistic therapeutic strategies have emerged as a powerful alternative, whereby PDT is combined with complementary modalities such as PTT,

chemotherapy, or immunotherapy. Such integrated approaches often yield superior efficacy compared to monotherapies by leveraging distinct mechanisms of action.

In this context, Li *et al.* developed a morpholine-functionalized BODIPY probe (**25**) capable of mediating both PDT and PTT for enhanced therapeutic outcomes (Fig. 29 and 31A, B).[103] The precursor BODIPY was synthesized *via* a Knoevenagel condensation with *N*,*N*-diethylaminobenzaldehyde under microwave-assisted conditions, which provided high yields and allowed recovery of unreacted starting materials. Subsequent C–N coupling, catalyzed by Pd$_2$(dba)$_3$ with BrettPhos as the ligand (noted for its superior efficiency over conventional triphenylphosphine ligands), resulted in the final probe **25**. The extended conjugation results in absorption and emission bands at 632 nm and 770 nm, respectively, and a quantum yield of 0.10. The probe **25** exhibited good singlet oxygen yield (ϕ_Δ of 2.4%) compared to MB (ϕ_Δ of 0.52% in DMSO)-PDT agent, high photostability, and photothermal efficiency of ∼23%. The probe specifically localized to lysosomes of cancer cells (HeLa and 4T1 cells), could generate ROS in cells under laser irradiation as a PDT agent to destroy lysosomal cancer cells, with low dark toxicity and sufficient phototoxicity (IC$_{50}$: 15.7 µM (HeLa), 11.6 µM (4T1)).
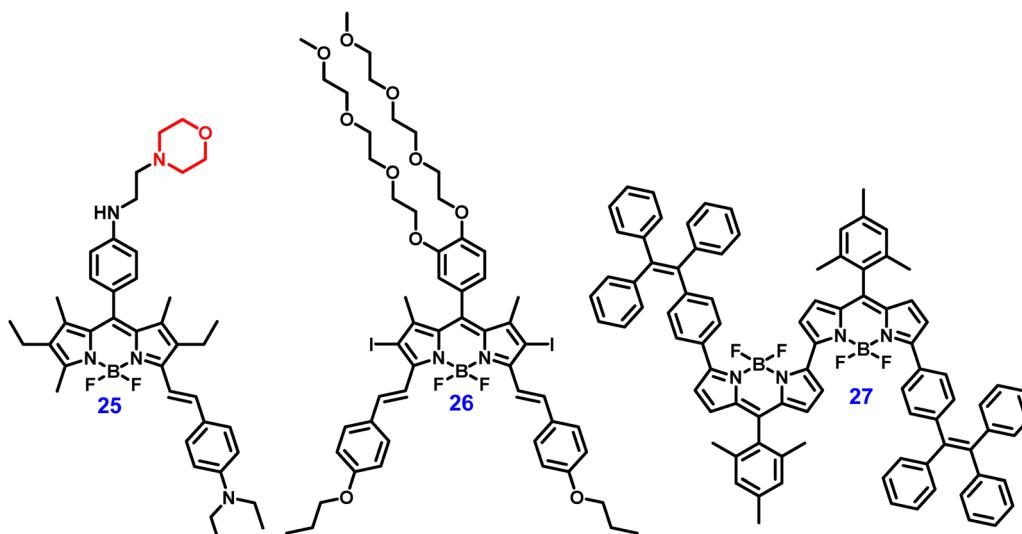

Fig. 29 Chemical structures of probes **25–27**. (Redrawn the ChemDraw structures from ref. 103–105).

This journal is © The Royal Society of Chemistry 2025

J. Mater. Chem. B, 2025, **13**, 12831–12868 | **12857**

Further, the *in vivo* studies conducted in mice tumor models also proved the effective tumor ablation without side effects (no necrosis/damage to other organs), underscoring the probe's therapeutic potential and biosafety for future clinical translation.

Meanwhile, Guo and co-workers reported amphiphilic J-aggregate-based BODIPY nanoparticles (**26**) for combined PDT and PTT therapy without the need for a specific lysosome-targeting moiety (Fig. 29, 30 and 31C).[104] The probe was synthesized by iodination of a BODIPY precursor followed by double Knoevenagel condensation with 4-propoxybenzaldehyde, and subsequently self-assembled into stable amphiphilic J-aggregates within PEG114-*b*-PCL60 polymeric micelles. Notably, micelles with 20% drug loading exhibited pronounced intermolecular π–π stacking and hydrophobic–hydrophilic interactions, resulting in red-shifted absorption (λ_{ab} = 730 nm) and quenched fluorescence (ϕ_F < 0.01) at 785 nm, facilitating efficient ROS and photothermal capacity under 785 nm irradiation (ϕ_Δ of 0.38, and PCE of 29%) and high photostability. The micelles showed high lysosomal uptake in 4T1 tumor cells *via* clathrin-mediated endocytic pathway and membrane disruption *via* photochemical translocation, with strong phototoxicity (IC_{50} = 16.2 µg mL^{-1}), minimal dark toxicity, and combination index (CI) of 0.71 under 785 nm irradiation. *In vivo* experiments confirmed strong tumor inhibition, affirming the dual PDT/PTT efficacy and biosafety of the system.

Further, Hao and colleagues developed another approach for lysosome-specific dual phototherapy by synthesizing α–α linked bisBODIPY NPs **27** (Fig. 29).[105] The design incorporates several key features: (1) two bulky tetraphenylethene (TPE) moieties at the α-positions of bisBODIPY extend the π-conjugation, affording strong NIR absorption (λ_{ab} = 742 nm) and emission (λ_{em} = 810 nm); (2) the molecular rotor nature of TPE enhances PCE and AIE, minimizing ROS quenching in aqueous environments; (3) the D–A architecture between TPE (donor) and BODIPY (acceptor) promotes ISC *via* enhanced spin–orbit coupling; (4) intra- and intermolecular J-type exciton coupling further facilitates ISC; and (5) incorporation of amphiphilic F-127 polymer enables nanoparticle formation with improved biocompatibility, lysosomal targeting, dispersion stability, and extended circulation time in blood. Compared to the commercial phototheraputic agent ICG, the probe **27** demonstrates markedly improved performance: (i) significantly enhanced ROS generation (including OH$^\bullet$ and $^1O_2$), with a 46.2-fold increase in both solution and 4T1 cells; (ii) a high PCE of 64.3% *versus* 25.4% for ICG; (iii) excellent photothermal stability over 10 laser on/off cycles without degradation (*versus* a single stable cycle for ICG); (iv) robust storage stability over two months; and (v) superior phototheraputic efficacy with low dark toxicity and high phototoxicity (IC_{50} in HeLa cells: ∼4.1 µM for the probe *vs.* ∼12.3 µM for ICG). *In vivo* studies further revealed effective tumor ablation and suppressed proliferation in mouse tumor models, underscoring the probe's therapeutic potential and biosafety for future clinical translation.

3.5.4 Combination therapies: PDT and photoacoustic imaging (PAI). Although fluorescence imaging in the NIR-I window (650–900 nm) effectively suppresses tissue autofluorescence, its penetration depth remains shallow (∼1 cm). To overcome this limitation, photoacoustic imaging (PAI) has emerged as a complementary modality, coupling the advantages of optical excitation with ultrasound detection to achieve deeper tissue penetration (5–6 cm) and higher spatial resolution. Therefore, Huang and co-workers pioneered the design of lysosome-acid-responsive bis-styryl BODIPY nanoparticles (**28**) that integrate both PDT and PAI functionalities (Fig. 32 and 33).[106] Designed with a D–π–A architecture, the probe incorporates a dimethylaminophenyl donor as an acid-sensitive group, with lysosomal selectivity and pH-activated PDT. This "switch-on" effect ensures that PDT is activated under acidic lysosomal conditions (pH 5.0–5.5) but suppressed at physiological pH, minimizing nonspecific phototoxicity. Encapsulation within DSPE-mPEG5000 produced hydrophilic and biocompatible nanoparticles with excellent chemical and physiological stability. Compared with the dye alone (λ_{ab} = 760 nm in DMF), probe **28** NPs exhibited slightly red-shifted absorption (λ_{ab} = 775 nm in aqueous solution) and superior photostability under continuous 730 nm irradiation, outperforming commercial ICG, which rapidly lost >80% of its absorption. Strong fluorescence quenching of the bis-styryl BODIPY dye within NPs generated robust PA signals under 730 nm laser irradiation (6.1 mJ cm^{-2}, well below ANSI safety limits), with lysosomal accumulation confirmed by six-fold higher PA signals
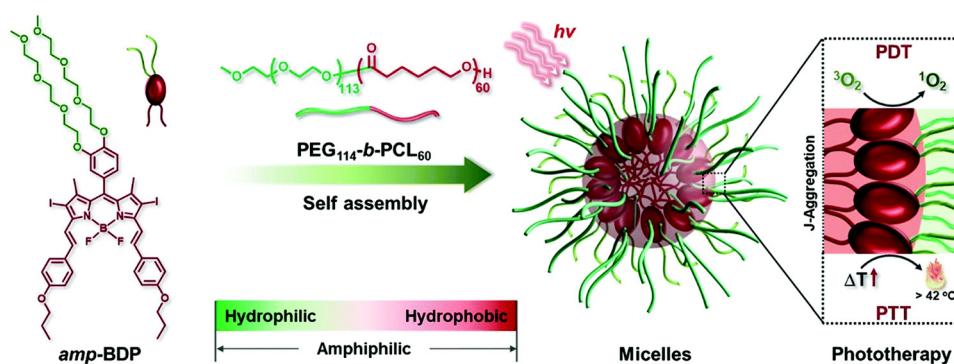

Fig. 30 Schematic illustration of probe **26** micelles designed for combined PDT and PTT. Reproduced with permission from ref. 104, Copyright 2020 Royal Society of Chemistry.

12858 | *J. Mater. Chem. B*, 2025, **13**, 12831–12868

This journal is © The Royal Society of Chemistry 2025
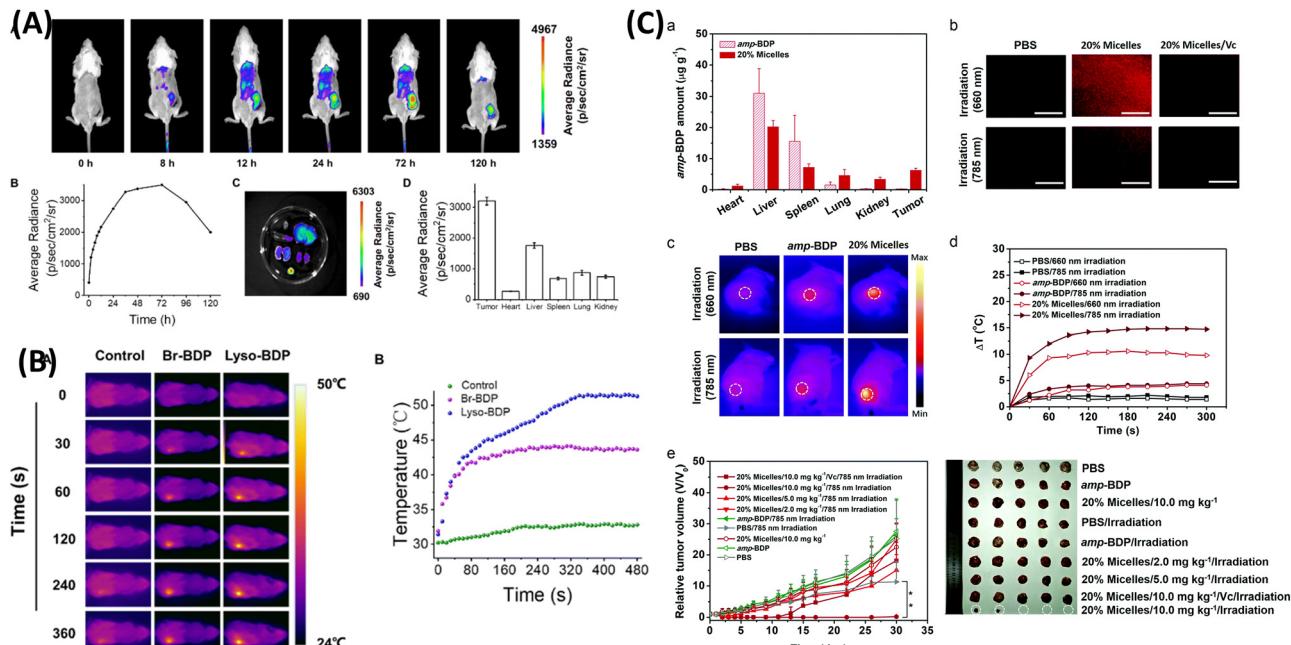
Fig. 31 (A) *In vivo* fluorescence imaging of tumor-bearing mice administered with probe **25** at different time intervals, highlighting its tumor-targeting capability. Reproduced with permission from ref. 103, Copyright 2023 Royal Society of Chemistry. (B) Confocal imaging of probe **25** in mice models under continuous laser irradiation, illustrating its application in PTT. Reproduced with permission from ref. 103. (C) *In vivo* studies of probe **26** (20% micelles) in mice bearing 4T1 tumors for photo-induced cancer therapy- (PDT and PTT). Reproduced with permission from ref. 104, Copyright 2020 Royal Society of Chemistry.
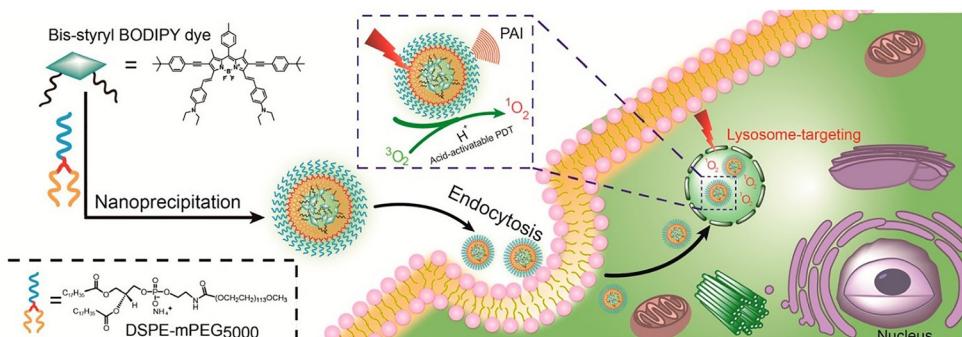

Fig. 32 Schematic representation of lysosome-targeting probe **28** NPs and their utility in both PAI and pH-activatable PDT under NIR light. Reproduced with permission from ref. 106, Copyright 2016 American Chemical Society.

in lysosomes relative to the cytoplasm. Functionally, probe **28** achieved significant PDT efficacy in A549 cells under 730 nm irradiation, reducing cell viability to 47.3% in acidic lysosomes, whereas ICG-treated cells remained viable, highlighting the superior acid-activated PDT effect. Annexin V-FITC/PI assays further demonstrated extensive apoptosis (87% apoptotic population) upon combined NP and laser treatment. *In vivo* studies in A549 tumor-bearing mice validated both the strong PAI performance and lysosome-activated PDT efficacy, confirming the potential of probe **28** as a highly efficient NIR theranostic agent for image-guided therapy.

3.5.5 Multimodal chemo-phototherapy. Recent studies have highlighted the potential of PDT to enhance chemotherapy, as the ROS generated during PDT can facilitate cellular

uptake of chemotherapeutic agents, accelerate drug release, and amplify cytotoxicity. Likewise, PTT not only induces hyperthermia to directly ablate tumor cells but also enhances tumor oxygenation, promotes drug delivery through accelerated blood flow, and increases membrane permeability, thereby improving intracellular drug accumulation. Consequently, the synergistic integration of chemotherapy with phototherapy (PDT and/or PTT) has emerged as a promising strategy, where the complementary mechanisms mutually reinforce each other to achieve superior antitumor efficacy compared to either modality alone. With this in mind, Yuan *et al.* designed and synthesized a multi-functional BODIPY probe **29** for treating hypoxia tumors *via* multimodal chemo-phototherapy to boost therapeutic response (Fig. 34 and 35).[107] The design comprised:

This journal is © The Royal Society of Chemistry 2025

*J. Mater. Chem. B*, 2025, **13**, 12831–12868 | **12859**
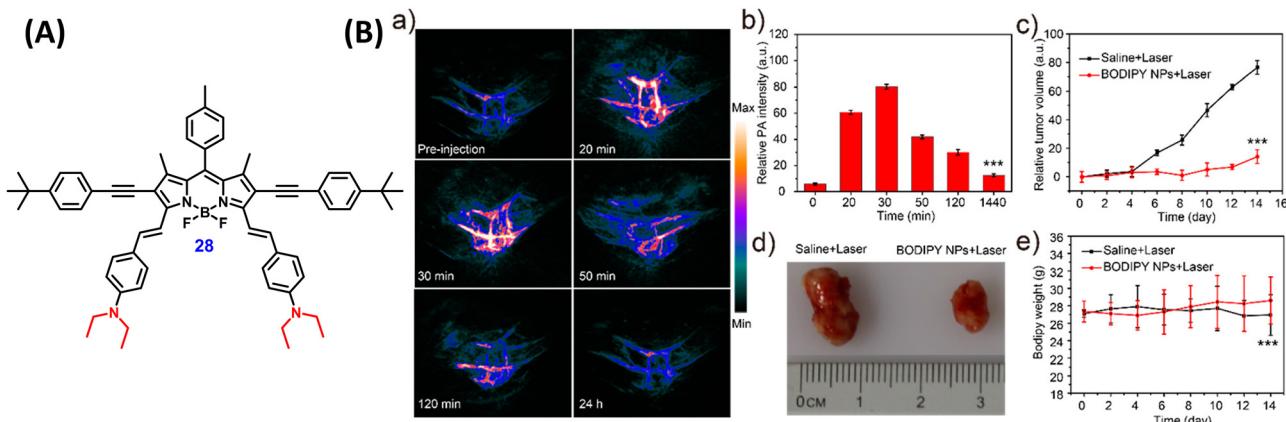
Fig. 33 (A) Chemical structure of probe **28**. (Redrawn the ChemDraw structures from ref. 106) (B) *in vivo* PAI of A549 tumor-bearing mice administered with probe **28** at a different time. Reproduced with permission from ref. 106, Copyright 2016 American Chemical Society.
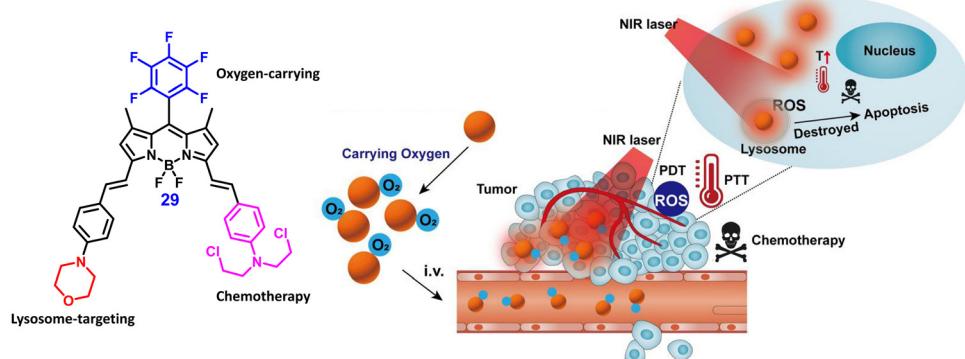
Fig. 34 Schematic representation of oxygen-carrying and lysosome-targeting NIR probe **29** for multimodal cancer therapy. Reproduced with permission from ref. 107, Copyright 2023 Elsevier.
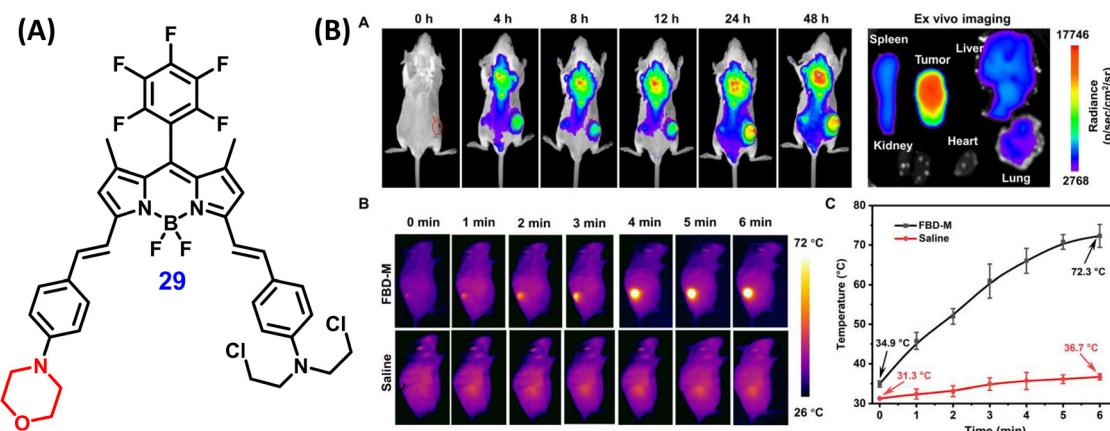
Fig. 35 (A) Chemical structure of probe **29**. (Redrawn the ChemDraw structures from ref. 107) (B) *in vivo* fluorescence imaging and infrared thermography of tumors following probe **29** administration, illustrating dual-modality functionality for tumor localization and photothermal monitoring under laser irradiation. Reproduced with permission from ref. 107, Copyright 2023 Elsevier.

(1) a BODIPY as the photoagent, (2) a pentafluorobenzene (acceptor) oxygen carrier to amplify PDT and drug release, (3) morpholine for lysosomal targeting, and (4) a nitrogen mustard moiety for chemotherapy. The probe exhibited NIR properties

(λ_{ab} = 731 nm, λ_{em} = 820 nm), excellent photostability with high PTT efficiency (PCE = 40.1%), moderate PDT yield (ϕ_Δ = 11.2%), O_2 carrying (13.28 mg L^{-1}), and loading (16.16 mg L^{-1}) capacity for alleviating tumour hypoxia. *In vitro* and *in vivo* studies in

12860 | *J. Mater. Chem. B*, 2025, **13**, 12831–12868

This journal is © The Royal Society of Chemistry 2025

HeLa and 4T1 models revealed low dark cytotoxicity, high phototoxicity (IC$_{50}$: 8.75 μM (HeLa), 10.02 μM (4T1)), and significant tumor inhibition (91.9% *vs.* control), establishing it as a promising platform for lysosome-targeted multimodal cancer therapy.

3.6 Challenges and future perspectives of lysosome-targeting probes

Despite notable advancements in the design of lysosome-targeted fluorescent probes, several critical challenges persist, limiting their broader applicability and precision in biological research:

1. Limited probe availability for various key biomolecules: although lysosomes play a vital role in cellular homeostasis and degradation processes, the available probes remain insufficient for many essential analytes. In particular, only a few have been developed for biologically significant species such as Ca^{2+}, Mg^{2+}, and various lysosomal hydrolases. The scarcity of effective analyte-responsive motifs, or incompatibility between the sensing moiety and lysosome-targeting units, hinders probe development. Expanding the probe library to target these reactive species represents a valuable direction for future research. In parallel, while some studies have explored the use of fluorescent proteins or nanomaterials to visualize lysosomal processes, especially autophagy approaches remain limited and could usefully complement small molecule probe strategies.

2. Targeting strategy-related lysosomal alkalization: most currently available lysosomal probes utilize lipophilic weakly basic groups for lysosomal targeting, relying on passive diffusion followed by protonation and accumulation within acidic compartments. However, prolonged exposure to such basic moieties can disrupt lysosomal pH homeostasis, leading to alkalization, impairment of lysosomal function, and eventual cell death. Additionally, these probes often display relative rather than absolute specificity; their basic anchors can accumulate in other acidic organelles, such as late endosomes, complicating subcellular localization and signal interpretation.

3. Enzymatic degradation and signal instability: the lysosomal environment is rich in hydrolytic enzymes capable of degrading small molecules, including fluorescent probes. This enzymatic activity can lead to the breakdown of probe structures, producing non-specific or false signals and compromising imaging accuracy in live-cell applications. As a result, designing probes with improved enzymatic stability remains an important challenge for achieving reliable and robust lysosomal detection.

4. False-positive signals due to pH sensitivity: many probes, particularly those used for metal ion detection, operate *via* PET mechanisms. Their recognition units often contain amine moieties, which can also interact with protons in the lysosomal environment, leading to undesired background fluorescence and false-positive results. This pH sensitivity restricts their specificity under physiologically relevant conditions.

5. Lack of probes for other digestive organelles: beyond lysosomes, other key components of the cellular digestive system, including early and late endosomes, autophagosomes, and autolysosomes, remain largely unexplored in terms of small-molecule fluorescent probe development. These organelles play vital roles in intracellular trafficking and degradation pathways. Probes designed to selectively target these compartments, potentially through mechanisms based on the endocytic or autophagic pathways, would significantly expand the toolkit available for studying intracellular degradation processes.

4 Lipid droplets (LDs) localized probes

4.1 Overview of LDs dynamics

Once regarded merely as inert storage sites for neutral lipids, LDs are now recognized as dynamic organelles actively involved in regulating cellular function and contributing to disease pathology.[108] They are found across nearly all life forms, from bacteria and yeast to plants and mammals, underscoring their essential biological roles.[109] Furthermore, their clear visualization under light microscopy emphasizes their widespread distribution and integral role in diverse cellular environments. Structurally, LDs possess a unique architecture that distinguishes them from other organelles.[110] They consist of a hydrophobic core composed predominantly of neutral lipids such as triglycerides, cholesteryl esters, and retinyl esters encased within a phospholipid monolayer embedded with a diverse set of proteins.[111,112] This differs markedly from the bilayer membrane and aqueous lumen characteristic of traditional membrane-bound organelles. These structural peculiarities enable LDs to adopt specialized functions and interaction patterns, including lipid synthesis, transport, and hydrolysis, energy homeostasis, and so on.[113] Their multifunctional nature positions LDs as central regulators of cellular lipid and protein homeostasis. Notably, LDs form highly dynamic inter-organelle contacts, especially with mitochondria, the endoplasmic reticulum, lysosomes, peroxisomes, and endosomes. These interactions facilitate the coordination of lipid exchange, metabolic integration, and stress response modulation, reinforcing the role of LDs as metabolic hubs.[113,114] The ability to adapt to environmental and metabolic cues underscores the importance of LDs in both normal physiology and disease contexts. Dysregulation of LD function or dynamics has been implicated in a broad range of metabolic and pathological disorders, including obesity, type 2 diabetes, non-alcoholic fatty liver disease, atherosclerosis, cardiovascular disease, and cancer.[112,115] In cancer, LDs play particularly complex and significant roles. Tumor cells often exhibit increased LD abundance, altered composition, and enhanced mobility, distinguishing them from non-malignant cells. Studies have shown that the density and motility of LDs correlate with tumor invasiveness and metastatic potential, suggesting that LDs could serve as valuable biomarkers for cancer diagnosis, prognosis, and treatment, further underscoring their relevance in precision oncology.[116]

4.2 General design rules for LDs probes

LDs composed of neutral lipid cores and a surrounding phospholipid monolayer represent a uniquely hydrophobic intracellular environment. As such, most LD-targeting fluorescent

This journal is © The Royal Society of Chemistry 2025

J. Mater. Chem. B, 2025, **13**, 12831–12868 | **12861**

probes rely on hydrophobic interactions to selectively accumulate within the LD core. These molecules tend to possess highly conjugated and lipophilic structures.[59] Without the need for a targeting moiety or specific binding mechanism, such dyes often undergo a solvatochromic shift and/or fluorescence turn-on in lipid-rich regions compared to the aqueous cellular environment. Widely used commercial probes such as Nile Red and BODIPY 493/503. While they offer a degree of lipid selectivity, each exhibits notable drawbacks: Nile Red displays green fluorescence in the presence of neutral lipids (*e.g.*, triglycerides) and red fluorescence in polar lipids (*e.g.*, phospholipids). However, it suffers from non-specific staining, particularly of intracellular membranes, and its broad emission spectrum leads to significant spectral overlap, complicating multicolor imaging. BODIPY 493/503 offers improved selectivity for neutral lipids and a narrower emission profile compared to Nile Red, but it can also non-specifically stain cellular membranes. Both dyes demonstrate poor photostability, small Stokes' shifts, and a low signal-to-noise ratio, limiting their suitability for long-term or high-contrast imaging.[114] These limitations underscore the need for next-generation LD probes with enhanced specificity, brightness, and photostability. To address the shortcomings of existing probes, the following factors should be prioritized in the design of new LD-targeting fluorophores:

1. Enhanced lipophilicity and structural bulkiness: increasing hydrophobicity improves localization within LD cores. Simultaneously, bulky structural motifs (*e.g.*, tetraphenylethylene) help reduce quenching caused by π–π stacking and limit nonspecific interactions.

2. Minimizing intramolecular hydrogen bonding: reducing intramolecular hydrogen bonding diminishes water affinity and enhances probe retention in LDs.

3. Fluorescence activation *via* microenvironmental triggers: probes incorporating microenvironment-responsive moieties (*e.g.*, HOCl-sensitive probes) can achieve turn-on fluorescence within LDs, enabling high contrast and specificity.

4. Photostability *via* AIE-active probes (AIEgens): are well-suited for LD imaging due to their enhanced emission in the aggregated state, while being quenched in solution. AIE dots also shield internal fluorophores from photooxidation, enhancing photostability and imaging duration.

4.3 Chemical routes to far-red/NIR LDs probes and their biomedical applicability

Given the critical biological functions of LDs, numerous LD-specific fluorescent probes have been developed using various fluorophore scaffolds. However, the majority of these probes lack emission in the NIR region, which limits their bioimaging performance due to low resolution, poor brightness, and suboptimal signal-to-noise ratios. To address these challenges, Jiao and co-workers recently designed a NIR-emissive BODIPY-based LD probe **30** by introducing sterically hindered tetraphenylethene (TPE) units at the 3,5-positions (α) and a mesityl group at the *meso*-position of the BODIPY core (Fig. 36).[117] This molecular design effectively suppresses π–π stacking interactions, mitigates ACQ, and promotes AIE, thereby shifting the emission into the NIR region. The resulting probe exhibited intense NIR fluorescence centered at 790 nm in the aggregated solid state, a substantial Stokes' shift of up to 130 nm, a high quantum yield ($\phi_F = 0.81$) in aqueous media, and excellent photostability. Notably, it demonstrated superior LD-targeting ability compared to the commercial BODIPY 493/503 dye and enabled real-time visualization of LD dynamics in live cells and the lipid-rich yolk sac of zebrafish larvae. Furthermore, the
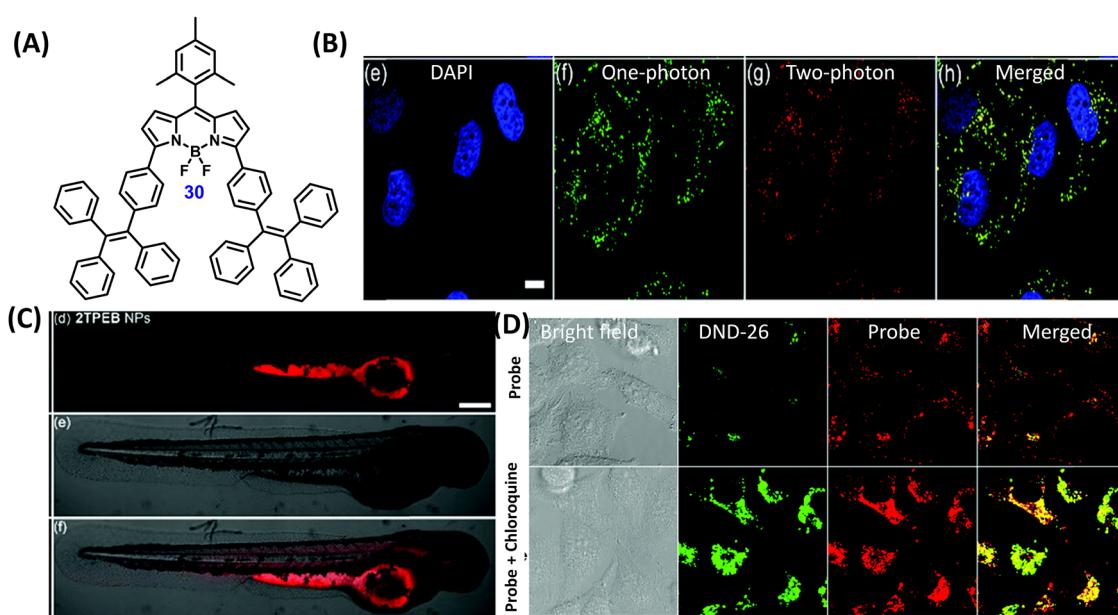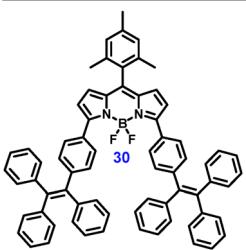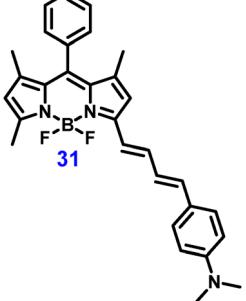
Fig. 36 (A) Chemical structure of probe **30**, (Redrawn the ChemDraw structure from ref. 117) (B) two-photon fluorescence images of probe **30** NPs in HeLa cells. (C) Confocal images of living zebrafish larvae stained with probe **30**. (D) Fluorescence images of HeLa cells before and after treatment with chloroquine. Reproduced with permission from ref. 117, Copyright 2021 Royal Society of Chemistry and Chinese Chemical Society.

12862 | *J. Mater. Chem. B*, 2025, **13**, 12831–12868

This journal is © The Royal Society of Chemistry 2025

Table 3 Summary of photophysical properties of LDs NIR BODIPY probes

Probes (P)	Analytes	Solvent	$\lambda_{ex}/\lambda_{em}$ (nm)	QY (ϕ_F)	Probe Conc/ dynamic range (μM)	LOD	Comments	Ref.
30	—	DCM	596/649	0.93	—	—	Real-time imaging of intracellular LD; monitoring of the LD-lysosome dynamics in living cells	117
31	Polarity	1,4 Dioxane and methanol	595/643 and 595/657	0.40 and 0.01	—	—	Polarity sensitive LD targeting probe for imaging LD polarity in contrast-induced AKI(CI-AKI) disease models	118

probe successfully facilitated imaging of LD-lysosome interactions, highlighting its potential utility in early disease diagnosis and therapeutic monitoring. A summary of the photophysical properties of LDs NIR BODIPY probes is given in Table 3.

Emerging evidence indicates that LD dysfunction may contribute to the onset of acute kidney injury (AKI). In a recent study, Zhou *et al.* reported the development of a LD-targeted NIR fluorescent probe **31** with high sensitivity to environmental polarity (Fig. 37 and 38).[118] The probe was constructed by conjugating a BODIPY core with 4-(dimethylamino)cinnamaldehyde, forming a (D–π–A) system. Due to TICT behavior, the probe exhibited weak fluorescence in highly polar solvents but showed significantly enhanced emission in non-polar environments, demonstrating polarity-dependent fluorescence with a linear response over the range of 0.0245 to 0.311. The probe also displayed favorable photophysical properties, including a large Stokes shift, high photostability, rapid response kinetics, low cytotoxicity, and excellent LD-targeting capability, along with a wash-free staining profile. Both *in vitro* and *in vivo*

experiments confirmed the probe's utility in visualizing LD polarity changes associated with contrast-induced AKI (CI-AKI). Notably, this study was the first to successfully monitor LD polarity fluctuations in live mice with CI-AKI using fluorescence imaging. Additionally, the probe preferentially accumulated in kidney tissue and it was also observed that normal cells exhibited higher polarity than cancer cells. These findings suggest the potential of this polarity-sensitive LD probe as a diagnostic and therapeutic marker for LD-related pathologies, particularly in conditions like CI-AKI where alterations in lipid microenvironments play a pivotal role.

4.4 Challenges and future perspectives of LDs probes

Despite advances, LD-specific *in vivo* probes, especially for therapeutic applications, remain underexplored. A major challenge lies in developing highly bright, NIR-emissive AIE probes capable of deep-tissue imaging with long-term photostability and minimal cytotoxicity. Expanding the chemical toolbox for novel targeting ligands specific to the LD membrane or surface proteins. Moreover, efficient strategies for LD targeting remain scarce, restricting detailed functional studies of lipid metabolism and signaling within these essential organelles.

(i) Designing activatable, environment-responsive probes with high brightness for monitoring dynamic cellular activities of LDs.

(ii) Integrating AIEgens into multifunctional nanostructures for combined imaging and therapy.

(iii) While current small-molecule probes primarily target the lipid core, the LD membrane itself presents opportunities for more targeted approaches. For instance, proteins such as perilipins are embedded in the phospholipid monolayer and could serve as selective anchors for probe binding. However,
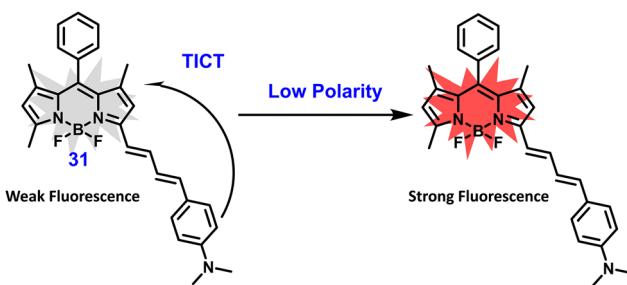

Fig. 37 Response mechanism of probe **31** to polarity. (Redrawn the ChemDraw structures from ref. 118).

This journal is © The Royal Society of Chemistry 2025

*J. Mater. Chem. B*, 2025, **13**, 12831–12868 | **12863**
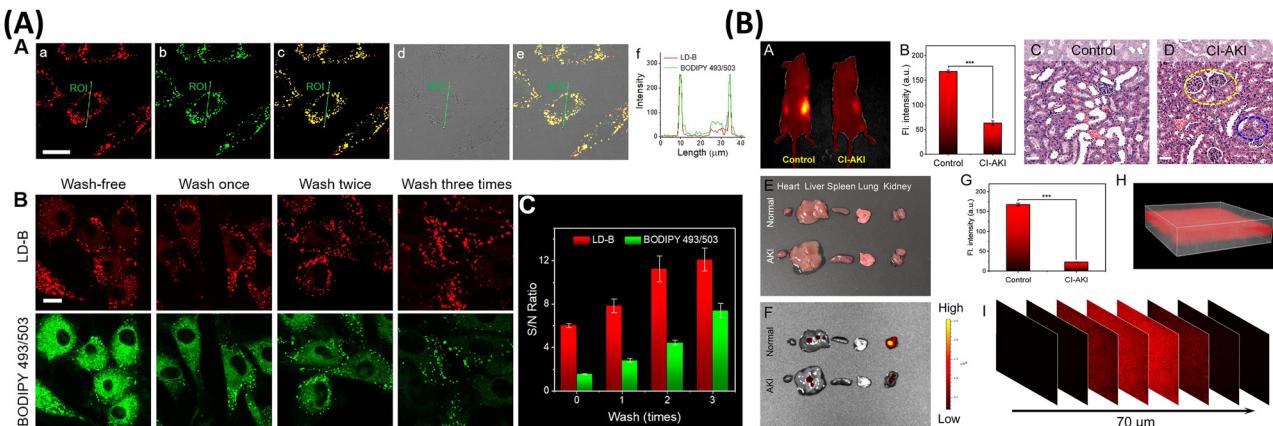
Fig. 38 (A) Confocal images of HBZY-1 cells treated with probe **31** and BODIPY 493/503-Co-localization images, without washing and after washing with PBS, S/N ratio *via* fluorescence intensity comparison. (B) *In vivo* images of probe **31** in normal BALB/c mice and AKI BALB/c mice. Reproduced with permission from ref. 118, Copyright 2023 American Chemical Society.

heterogeneous expression of these proteins within a single cell presents a challenge for universal probe design.[111]

5 Design strategies for NIR-II BODIPY fluorophores in advanced biomedical applications

The second near-infrared window (NIR-II, 1000–1700 nm) offers unique advantages over the NIR-I region, including ultra-low photon scattering, deep tissue penetration, and high spatial resolution. Despite these promising optical characteristics, the development of BODIPY-based NIR-II fluorophores, especially those tailored for organelle-specific targeting and therapeutic applications, remains scarce. This section outlines emerging design strategies aimed at extending the photophysical properties of BODIPY dyes into the NIR-II region while enhancing their functional relevance for biomedical use.[119]

1. Electron programming strategy: to achieve a mic shift in the absorption and emission spectra of the parent BODIPY scaffold into the NIR-II region, electron-donating moieties are strategically introduced. These include groups such as 4-julolidinyl, 4-anisoyl, and 4-(*N,N*-dimethylamino)phenyl, which are conjugated to the electron-deficient BODIPY core. This D–A interaction facilitates ICT, effectively narrowing the HOMO–LUMO energy gap and pushing the emission wavelength beyond 1000 nm.

2. Conjugation with semiconducting polymers: coupling BODIPY derivatives with semiconducting polymers especially those incorporating degradable segments, enables the formation of a large π-conjugated delocalized backbone. This hybrid design imparts superior optical properties, including strong NIR absorption, enhanced photothermal conversion, and controlled biodegradability, making these systems well-suited for image-guided therapy and diagnostics.

3. Formation of J-aggregates: the formation of J-aggregates represents an effective strategy to tune the optical properties of BODIPY derivatives, since they exhibit red-shifted absorption and emission, high fluorescence quantum yield, and enhanced

photostability. Basically, 4 strategies for J-aggregate formation: (a) introducing bulky steric hindrance, (b) regulating hydrogen bond (inter) interaction, (c) modulating hydrophilic/hydrophobic interaction, and (d) electronic regulation or molecular exciton coupling. For example, the introduction of electron-deficient groups (*e.g.*, nitro substituents) into the BODIPY framework promotes intermolecular hydrogen bonding and electrostatic interactions, facilitating J-aggregate formation and enhancing NIR-II fluorescence. However, a key challenge remains, including achieving controlled, *in situ* J-aggregation in complex biological environments, which often hampers the therapeutic applicability.

4. Development of activatable NIR-II fluorophores: to address the need for highly specific imaging with minimal background interference, activatable BODIPY-based NIR-II probes have emerged as a promising class. These fluorophores remain "off" under physiological conditions and are "turned on" upon interaction with specific analytes or environmental triggers. This is typically achieved by incorporating electron-deficient or fluorescence-quenching groups into the BODIPY core, rendering the molecule initially non-fluorescent. Upon encountering the target stimulus (*e.g.*, ROS, pH, enzymatic activity), the quenching is relieved, restoring fluorescence and enabling targeted imaging with high signal-to-background ratios.

While these strategies represent significant progress, the rational design of organelle-specific, NIR-II emissive BODIPY probes still poses synthetic and functional challenges, particularly in balancing optical performance, targeting precision, and *in vivo* stability. Nevertheless, the synergistic integration of electron modulation, aggregation control, polymer conjugation, and stimulus-responsiveness holds considerable promise for expanding the biomedical utility of BODIPY fluorophores in precision diagnostics and phototheranostics within the NIR-II window.

6 Conclusions and future perspectives

Subcellular organelles are integral to maintaining cellular homeostasis, and their dysfunction is linked to numerous

12864 | *J. Mater. Chem. B*, 2025, **13**, 12831–12868

This journal is © The Royal Society of Chemistry 2025

diseases, including cancer and neurodegenerative disorders. Therefore, precise targeting of therapeutics to specific organelles can enhance therapeutic efficacy by optimizing dosage thresholds, reducing toxicity, and minimizing off-target effects. In this context, BODIPY-based far-red/NIR fluorophores have demonstrated significant potential. Their tunable photophysical properties, high quantum efficiency, excellent photostability, and synthetic versatility render them ideal for subcellular imaging. Furthermore, their emission in the far-red/NIR region improves tissue penetration, reduces background autofluorescence, and facilitates real-time observation in complex biological environments. Their ability to integrate high-resolution imaging with localized therapeutic interventions, such as PDT, PTT, and combined therapies, boosts the potential of fluorescence-guided precision medicine.

In this review, we have highlighted the potential of BODIPY fluorophores as advanced molecular tools for subcellular imaging and theranostics. We placed particular emphasis on criteria for organelle-specific targeting, considering both physicochemical factors and structural design principles. Our primary focus was a critical evaluation of recent studies on far-red/NIR-emitting BODIPY-based probes designed for mitochondria, lysosomes, and lipid droplets. We investigated probe designs that enhance target specificity, photostability, and responsiveness to bioactive species and local microenvironmental factors, such as pH, polarity, and ROS. Beyond diagnostics, we reviewed the expanding use of BODIPY-based probes in phototherapy, particularly PDT, PTT, and their combined applications, including insights into *in vivo* performance and translational potential.

Despite these promising advancements, critical challenges remain, particularly in the systematic design of organelle-specific NIR fluorophores optimized for *in vivo* imaging and clinical use. Firstly, most current probes exhibit limited performance in the NIR-II window (1000–1700 nm), where superior imaging depth, resolution, and signal-to-noise ratios can be achieved. Secondly, pharmacokinetic challenges such as poor water solubility, nonspecific accumulation, and rapid systemic clearance reduce probe biocompatibility and hinder organelle-specific localization. Thirdly, biological complexities, including tumor heterogeneity, dynamic microenvironments, and enzymatic degradation, further compromise imaging accuracy and therapeutic selectivity. Lastly, concerns about long-term safety, biocompatibility, and immunogenicity remain significant obstacles to clinical translation.

To address these challenges, several strategies are emerging. Rational molecular engineering can extend BODIPY emission into the NIR-II region, enhance brightness, improve quantum yield, and incorporate ratiometric or activatable ("off–on") signaling modes.[18] Bioengineering approaches, including biodegradable nanocarriers, self-assembling small-molecule systems, and stimuli-responsive delivery platforms, can improve probe stability, enhance organelle accumulation, and prolong circulation time.[120] Computational approaches, particularly machine learning and AI, offer powerful tools for predicting structure–activity relationships, optimizing targeting motifs, and streamlining probe design.[121] These synergistic strategies can accelerate the development of next-generation probes with enhanced optical, pharmacological, and biological performance.

Looking forward, the most promising direction lies in the development of multifunctional, multi-responsive, and organelle-specific BODIPY probes.[121,122] Such probes could integrate diagnostics and therapy into a single platform, enabling simultaneous disease detection, monitoring, and intervention. Incorporation of biomarker-reactive motifs would facilitate highly selective activation within diseased cells, minimizing off-target effects. Dual- and multi-responsive designs capable of responding to pH, redox state, enzymatic activity, or reactive oxygen/nitrogen species could provide comprehensive readouts of organelle function and disease progression. Furthermore, probes capable of sequential or simultaneous multi-organelle imaging will help unravel the crosstalk between subcellular structures, offering deeper insights into the mechanisms of pathogenesis.

Equally important is the integration of BODIPY fluorophores with advanced imaging modalities. Two-photon and multiphoton microscopy, super-resolution imaging, and light-sheet fluorescence microscopy are already pushing the frontiers of deep-tissue and high-resolution imaging.[35] When combined with NIR-II responsive probes, these modalities can achieve unprecedented spatiotemporal resolution. Hybrid techniques such as photoacoustic imaging, positron emission tomography (PET), or Raman spectroscopy promise to expand diagnostic capabilities further by providing complementary structural, molecular, and functional information. Together, these multimodal platforms could significantly enhance disease diagnosis, monitoring, and treatment planning. In short, the convergence of rational molecular design, bioengineering innovation, computational intelligence, and advanced imaging technologies is poised to transform BODIPY-based organelle-targeted probes into clinically viable tools for precision medicine. By addressing current limitations and embracing multifunctional, multi-responsive designs, the next generation of BODIPY probes will integrate diagnostics with therapeutic interventions, enable real-time monitoring of treatment outcomes, and ultimately improve patient-specific healthcare. We anticipate that the roadmap outlined in this review will not only inspire further innovation in BODIPY probe design but also accelerate their journey from laboratory research to translational applications in personalized medicine.

Conflicts of interest

The authors declare no competing financial interest.

Data availability

No primary research results, software, or code have been included, and no new data were generated or analysed as part of this review.

Acknowledgements

This journal is © The Royal Society of Chemistry 2025

J. Mater. Chem. B, 2025, **13**, 12831–12868 | **12865**

References

1 A. Kar, S. Agarwal, A. Singh, A. Bajaj and U. Dasgupta, *Transl. Oncol.*, 2024, **42**, 101901.

2 J. E. Bennett, G. A. Stevens, C. D. Mathers, R. Bonita, J. Rehm, M. E. Kruk, L. M. Riley, K. Dain, A. P. Kengne, K. Chalkidou, J. Beagley, S. P. Kishore, W. Chen, S. Saxena, D. W. Bettcher, J. T. Grove, R. Beaglehole and M. Ezzati, *Lancet*, 2018, **392**, 1072–1088.

3 K. Wang and J. E. Tepper, *Ca-Cancer J. Clin.*, 2021, **71**, 437–454.

4 Y. Li, Y. Chen, W. Pan, Z. Yu, L. Yang, H. Wang, N. Li and B. Tang, *Nanoscale*, 2017, **9**, 17318–17324.

5 M. S. De Almeida, E. Susnik, B. Drasler, P. Taladriz-Blanco, A. Petri-Fink and B. Rothen-Rutishauser, *Chem. Soc. Rev.*, 2021, **50**, 5397–5434.

6 X. Wan, X. Zhang, W. Pan, B. Liu, L. Yu, H. Wang, N. Li and B. Tang, *Anal. Chem.*, 2019, **91**, 6088–6096.

7 A. Saminathan, M. Zajac, P. Anees and Y. Krishnan, *Nat. Rev. Mater.*, 2021, **7**, 355–371.

8 J. Soukar, N. A. Peppas and A. K. Gaharwar, *Adv. Sci.*, 2025, **12**, 2411720–2411736.

9 D. Singh, *Endocr., Metab. Immune Disord.:Drug Targets*, 2024, **24**, 1480–1487.

10 J. Yang, A. Griffin, Z. Qiang and J. Ren, *Signal Transduction Targeted Ther.*, 2022, **7**, 379.

11 A. A. Khan, K. S. Allemailem, A. Almatroudi, S. A. Almatroodi, M. A. Alsahli and A. H. Rahmani, *J. Drug Delivery Sci. Technol.*, 2020, **61**, 102315–102330.

12 Y. Yan, Y. Zhang, J. Liu, B. Chen and Y. Wang, *Med. Rev.*, 2024, **5**, 117–138.

13 J. Parker, *Annu. Rev. Cell Dev. Biol.*, 2024, **40**, 51–74.

14 Y. Li, Y. Liu, X.-Y. Yu, Y. Xu, X. Pan, Y. Sun, Y. Wang, Y.-H. Song and Z. Shen, *Signal Transduction Targeted Ther.*, 2024, **9**, 305.

15 E. Burbridge and C. Adrain, *FEBS J.*, 2022, **289**, 6822–6831.

16 P. Gao, W. Pan, N. Li and B. Tang, *Chem. Sci.*, 2019, **10**, 6035–6071.

17 H. Zhu, J. Fan, J. Du and X. Peng, *Acc. Chem. Res.*, 2016, **49**, 2115–2126.

18 W. Xu, Z. Zeng, J. Jiang, Y. Chang and L. Yuan, *Angew. Chem., Int. Ed.*, 2016, **55**, 13658–13699.

19 X. Jiao, Y. Li, J. Niu, X. Xie, X. Wang and B. Tang, *Anal. Chem.*, 2017, **90**, 533–555.

20 W. Chen, H. Zhao and Y. Li, *Signal Transduction Targeted Ther.*, 2023, **8**, 333.

21 Z. Xu and L. Xu, *Chem. Commun.*, 2015, **52**, 1094–1119.

22 R. Liu, W. Hong, D. Hou, H. Huang and C. Duan, *Adv. Biol.*, 2024, **8**, 2300288–2300301.

23 G. S. Attar, M. Kumar and V. Bhalla, *Chem. Commun.*, 2024, **60**, 11610–11624.

24 M. Dirak, C. M. Yenici and S. Kolemen, *Coord. Chem. Rev.*, 2024, **506**, 215710–215735.

25 E. Hwang and H. S. Jung, *Chem. Commun.*, 2021, **57**, 7731–7742.

26 H. Liu and H. Wang, *Adv. Drug Delivery Rev.*, 2024, **209**, 115327–115341.

27 H. Yu and M. Ji, *Mol. Imaging Biol.*, 2020, **23**, 160–172.

28 C. Li, G. Chen, Y. Zhang, F. Wu and Q. Wang, *J. Am. Chem. Soc.*, 2020, **142**, 14789–14804.

29 J. W. Lichtman and J.-A. Conchello, *Nat. Methods*, 2005, **2**, 910–919.

30 M. Schäferling, *Angew. Chem., Int. Ed.*, 2012, **51**, 3532–3554.

31 Y. Yang, Q. Zhao, W. Feng and F. Li, *Chem. Rev.*, 2012, **113**, 192–270.

32 Z. Yang, J. Cao, Y. He, J. H. Yang, T. Kim, X. Peng and J. S. Kim, *Chem. Soc. Rev.*, 2014, **43**, 4563–4601.

33 Z. Guo, S. Park, J. Yoon and I. Shin, *Chem. Soc. Rev.*, 2013, **43**, 16–29.

34 C. Ding and T. Ren, *Coord. Chem. Rev.*, 2023, **482**, 215080.

35 P. Liu, X. Mu, X.-D. Zhang and D. Ming, *Bioconjugate Chem.*, 2019, **31**, 260–275.

36 Y. Liu, Y. Li, S. Koo, Y. Sun, Y. Liu, X. Liu, Y. Pan, Z. Zhang, M. Du, S. Lu, X. Qiao, J. Gao, X. Wang, Z. Deng, X. Meng, Y. Xiao, J. S. Kim and X. Hong, *Chem. Rev.*, 2021, **122**, 209–268.

37 C. Li, X. Guan, X. Zhang, D. Zhou, S. Son, Y. Xu, M. Deng, Z. Guo, Y. Sun and J. S. Kim, *Biosens. Bioelectron.*, 2022, **216**, 114620.

38 D. Ma, H. Bian, M. Gu, L. Wang, X. Chen and X. Peng, *Coord. Chem. Rev.*, 2024, **505**, 215677–215703.

39 T. Kowada, H. Maeda and K. Kikuchi, *Chem. Soc. Rev.*, 2015, **44**, 4953–4972.

40 S. Samanta, K. Lai, F. Wu, Y. Liu, S. Cai, X. Yang, J. Qu and Z. Yang, *Chem. Soc. Rev.*, 2023, **52**, 7197–7261.

41 S. Das, S. Dey, S. Patra, A. Bera, T. Ghosh, B. Prasad, K. D. Sayala, K. Maji, A. Bedi and S. Debnath, *Biomolecules*, 2023, **13**, 1723–1739.

42 N. A. Bumagina and E. V. Antina, *Coord. Chem. Rev.*, 2024, **505**, 215688–215730.

43 M. Poddar and R. Misra, *Coord. Chem. Rev.*, 2020, **421**, 213462–213483.

44 P. P. P. Kumar, S. Saxena and R. Joshi, *Colorants*, 2025, **4**, 13.

45 H. Ahmad, S. Muhammad, M. Mazhar, A. Farhan, M. S. Iqbal, H. Hiria, C. Yu, Y. Zhang and B. Guo, *Coord. Chem. Rev.*, 2024, **526**, 216383–216427.

46 V. I. Martynov and A. A. Pakhomov, *Russ. Chem. Rev.*, 2021, **90**, 1213–1262.

47 G. Y. Wiederschain, *Biochemistry*, 2011, **76**, 1276.

48 A. Treibs and F. Kreuzer, *Justus Liebigs Ann. Chem.*, 1968, **718**, 208–223.

49 A. Loudet and K. Burgess, *Chem. Rev.*, 2007, **107**, 4891–4932.

50 I. S. Yadav and R. Misra, *J. Mater. Chem. C*, 2023, **11**, 8688–8723.

51 Y. Ni and J. Wu, *Org. Biomol. Chem.*, 2014, **12**, 3774–3791.

52 Z. Shi, X. Han, W. Hu, H. Bai, B. Peng, L. Ji, Q. Fan, L. Li and W. Huang, *Chem. Soc. Rev.*, 2020, **49**, 7533–7567.

53 L. Bai, P. Sun, Y. Liu, H. Zhang, W. Hu, W. Zhang, Z. Liu, Q. Fan, L. Li and W. Huang, *Chem. Commun.*, 2019, **55**, 10920–10923.

12866 | *J. Mater. Chem. B*, 2025, **13**, 12831–12868

This journal is © The Royal Society of Chemistry 2025

54 H. Li, J. Wang, L. Jiao and E. Hao, *Chem. Commun.*, 2024, **60**, 5770–5789.

55 B. Cheng, V. Bandi, S. Yu, F. D'Souza, K. T. Nguyen, Y. Hong, L. Tang and B. Yuan, *Int. J. Mol. Sci.*, 2017, **18**, 384–397.

56 Z. Lei and F. Zhang, *Angew. Chem., Int. Ed.*, 2020, **60**, 16294–16308.

57 G. Jiang, H. Liu, H. Liu, G. Ke, T. Ren, B. Xiong, X. Zhang and L. Yuan, *Angew. Chem., Int. Ed.*, 2024, **63**, e202315217.

58 X. Feng, L. Wei, Y. Liu, X. Chen and R. Tian, *Adv. Healthcare Mater.*, 2023, **12**, 2300537–2300560.

59 S. H. Alamudi and Y.-A. Lee, *RSC Adv.*, 2025, **15**, 2115–2131.

60 J. Lin, K. Yang and E. J. New, *Org. Biomol. Chem.*, 2021, **19**, 9339–9357.

61 M. Zhu, W. Li, L. Sun, Z. Lv, X. Yang and Y. Wang, *Coord. Chem. Rev.*, 2024, **512**, 215893–215916.

62 S. Lu, Z. Dai, Y. Cui and D.-M. Kong, *Biosensors*, 2023, **13**, 360–387.

63 N.-E. Choi, J.-Y. Lee, E.-C. Park, J.-H. Lee and J. Lee, *Molecules*, 2021, **26**, 217–235.

64 C. Ma, F. Xia and S. O. Kelley, *Bioconjugate Chem.*, 2020, **31**, 2650–2667.

65 Q. Ding, X. Wang, Y. Luo, X. Leng, X. Li, M. Gu and J. S. Kim, *Coord. Chem. Rev.*, 2024, **508**, 215772–215796.

66 H. Wang, B. Fang, B. Peng, L. Wang, Y. Xue, H. Bai, S. Lu, N. H. Voelcker, L. Li, L. Fu and W. Huang, *Front. Chem.*, 2021, **9**, 683220.

67 S. Samanta, Y. He, A. Sharma, J. Kim, W. Pan, Z. Yang, J. Li, W. Yan, L. Liu, J. Qu and J. S. Kim, *Chem*, 2019, **5**, 1697–1726.

68 H. Crawford, M. Dimitriadi, J. Bassin, M. T. Cook, T. F. Abelha and J. Calvo-Castro, *Chem. – Eur. J.*, 2022, **28**, e202202366.

69 B. Glancy, Y. Kim, P. Katti and T. B. Willingham, *Front. Physiol.*, 2020, **11**, 541040.

70 S. Wang, L. Gai, Y. Chen, X. Ji, H. Lu and Z. Guo, *Chem. Soc. Rev.*, 2024, **53**, 3976–4019.

71 N. Jiang, J. Fan, T. Liu, J. Cao, B. Qiao, J. Wang, P. Gao and X. Peng, *Chem. Commun.*, 2013, **49**, 10620–10622.

72 J.-L. Wang, L. Zhang, L.-X. Gao, J.-L. Chen, T. Zhou, Y. Liu and F.-L. Jiang, *J. Mater. Chem. B*, 2021, **9**, 8639–8645.

73 X. Zhang, Y. Xiao, J. Qi, J. Qu, B. Kim, X. Yue and K. D. Belfield, *J. Org. Chem.*, 2013, **78**, 9153–9160.

74 J. Yang, R. Zhang, Y. Zhao, J. Tian, S. Wang, C. P. Gros and H. Xu, *Spectrochim. Acta, Part A*, 2021, **248**, 119199.

75 X. Song, S. Bai, N. He, R. Wang, Y. Xing, C. Lv and F. Yu, *ACS Sens.*, 2021, **6**, 1228–1239.

76 B.-X. Shen, Y. Qian, Z.-Q. Qi, C.-G. Lu, Q. Sun, X. Xia and Y.-P. Cui, *J. Mater. Chem. B*, 2017, **5**, 5854–5861.

77 Y. Huang, X. Zhang, N. He, Y. Wang, Q. Kang, D. Shen, F. Yu and L. Chen, *J. Mater. Chem. B*, 2019, **7**, 305–313.

78 M. Gao, F. Yu, H. Chen and L. Chen, *Anal. Chem.*, 2015, **87**, 3631–3638.

79 M. Gao, R. Wang, F. Yu and L. Chen, *Biomaterials*, 2018, **160**, 1–14.

80 L. Wang, J. Wang, S. Xia, X. Wang, Y. Yu, H. Zhou and H. Liu, *Talanta*, 2020, **219**, 121296.

81 S.-J. He, Y.-W. Xie and Q.-Y. Chen, *Spectrochim. Acta, Part A*, 2018, **195**, 210–214.

82 H. Agarwalla, P. S. Mahajan, D. Sahu, N. Taye, B. Ganguly, S. B. Mhaske, S. Chattopadhyay and A. Das, *Inorg. Chem.*, 2016, **55**, 12052–12060.

83 W.-J. Shi, Y.-F. Wei, J. Yang, H.-Z. Li, Q.-H. Wan, Y. Wang, H. Leng, K. Chen and J.-W. Yan, *Sens. Actuators, B*, 2022, **359**, 131594.

84 I. W. Badon, C. Kim, J. M. Lim, D. K. Mai, T. P. Vales, D. Kang, S. Cho, J. Lee, H.-J. Kim and J. Yang, *J. Mater. Chem. B*, 2022, **10**, 1196–1209.

85 W.-W. Xiao, S. Chen, M.-X. Liu and Y.-L. Yu, *Chem. Commun.*, 2025, **61**, 7929–7944.

86 M. Cao, X. Luo, K. Wu and X. He, *Signal Transduction Targeted Ther.*, 2021, **6**, 379.

87 S. R. Bonam, F. Wang and S. Muller, *Nat. Rev. Drug Discovery*, 2019, **18**, 923–948.

88 J.-L. Zhu, Z. Xu, Y. Yang and L. Xu, *Chem. Commun.*, 2019, **55**, 6629–6671.

89 X. Duan, Q. Tong, C. Fu and L. Chen, *Bioorg. Chem.*, 2023, **140**, 106832.

90 N. Mukherjee, R. Gaur, S. Shahabuddin and P. Chandra, *Mater. Today: Proc.*, 2022, **62**, 7082–7087.

91 B. Rathore, K. Sunwoo, P. Jangili, J. Kim, J. H. Kim, M. Huang, J. Xiong, A. Sharma, Z. Yang, J. Qu and J. S. Kim, *Biomaterials*, 2019, **211**, 25–47.

92 Y. He, S. Wang, P. Yu, K. Yan, J. Ming, C. Yao, Z. He, A. M. El-Toni, A. Khan, X. Zhu, C. Sun, Z. Lei and F. Zhang, *Chem. Sci.*, 2021, **12**, 10474–10482.

93 Z. Ye, C. Xiong, J. Pan, D. Su and L. Zeng, *Dyes Pigm.*, 2018, **155**, 30–35.

94 M. Grossi, M. Morgunova, S. Cheung, D. Scholz, E. Conroy, M. Terrile, A. Panarella, J. C. Simpson, W. M. Gallagher and D. F. O'Shea, *Nat. Commun.*, 2016, **7**, 10855.

95 J. Zhang, M. Yang, C. Li, N. Dorh, F. Xie, F.-T. Luo, A. Tiwari and H. Liu, *J. Mater. Chem. B*, 2015, **3**, 2173–2184.

96 J. Zhang, S. Gong, Q. Li, S. Zhang and G. Feng, *Anal. Chem.*, 2024, **96**, 14053–14059.

97 Y. Liang, C. Zhang, Z. Meng, S. Gong, J. Tian, R. Li, Z. Wang and S. Wang, *Sens. Actuators, B*, 2024, **417**, 136044.

98 C. Ma, J. Wu, W. Sun, Y. Hou, G. Zhong, R. Gao, B. Shen and H. Huang, *Sens. Actuators, B*, 2020, **325**, 128798.

99 X. Kong, L. Di, Y. Fan, Z. Zhou, X. Feng, L. Gai, J. Tian and H. Lu, *Chem. Commun.*, 2019, **55**, 11567–11570.

100 M. Li, R. Tian, J. Fan, J. Du, S. Long and X. Peng, *Dyes Pigm.*, 2017, **147**, 99–105.

101 Q. Wang, D. K. P. Ng and P.-C. Lo, *J. Mater. Chem. B*, 2018, **6**, 3285–3296.

102 Z. Kang, W. Bu, X. Guo, L. Wang, Q. Wu, J. Cao, H. Wang, C. Yu, J. Gao, E. Hao and L. Jiao, *Inorg. Chem.*, 2024, **63**, 3402–3410.

103 Y. Liu, J. Gao, H. Li, M. Yang, J. Lv, Y. Zhou, Z. Yuan and X. Li, *Org. Biomol. Chem.*, 2023, **21**, 4672–4682.

104 Z. Yan, M. Wang, M. Shi, Y. He, Y. Zhang, S. Qiu, H. Yang, H. Chen, H. He and Z. Guo, *J. Mater. Chem. B*, 2020, **8**, 6886–6897.

This journal is © The Royal Society of Chemistry 2025

J. Mater. Chem. B, 2025, **13**, 12831–12868 | **12867**

105 X. Guo, B. Tang, Q. Wu, W. Zhong, Q. Gong, S. Ling, L. Jiao, X. Jiang and E. Hao, *ACS Appl. Mater. Interfaces*, 2024, **16**, 41916–41926.

106 W. Hu, H. Ma, B. Hou, H. Zhao, Y. Ji, R. Jiang, X. Hu, X. Lu, L. Zhang, Y. Tang, Q. Fan and W. Huang, *ACS Appl. Mater. Interfaces*, 2016, **8**, 12039–12047.

107 J. Gao, T. Luan, J. Lv, M. Yang, H. Li and Z. Yuan, *J. Photochem. Photobiol., B*, 2023, **241**, 112666.

108 R. V. J. Farese and T. C. Walther, *Cell*, 2009, **139**, 855–860.

109 T. Fujimoto, Y. Ohsaki, J. Cheng, M. Suzuki and Y. Shinohara, *Histochem. Cell Biol.*, 2008, **130**, 263–279.

110 Y. Jin, Y. Tan, J. Wu and Z. Ren, *Cell Death Discovery*, 2023, **9**, 254.

111 J. A. Olzmann and P. Carvalho, *Nat. Rev. Mol. Cell Biol.*, 2019, **20**, 137–155.

112 A. Zadoorian, X. Du and H. Yang, *Nat. Rev. Endocrinol.*, 2023, **19**, 443–459.

113 (*a*) M. Gao, X. Huang, B.-L. Song and H. Yang, *Prog. Lipid Res.*, 2019, **75**, 100989–100999; (*b*) M. F. Renne and H. Hariri, *Front. Cell Dev. Biol.*, 2021, **9**, 726261–726271; (*c*) J. Z. Hsia, D. Liu, L. Haynes, R. Cruz-Cosme and Q. Tang, *Microorganisms*, 2024, **12**, 647–670.

114 Y.-X. Zhou, S.-Y. Wu, X. Zhang and F.-G. Wu, *Anal. Chem.*, 2024, **175**, 117703–117729.

115 B. C. Farmer, A. E. Walsh, J. C. Kluemper and L. A. Johnson, *Front. Neurosci.*, 2020, **14**, 742–754.

116 A. L. S. Cruz, E. A. Barreto, N. P. B. Fazolini, J. P. B. Viola and P. T. Bozza, *Cell Death Dis.*, 2020, **11**, 105–120.

117 X. Guo, B. Tang, H. Wu, Q. Wu, Z. Xie, C. Yu, E. Hao and L. Jiao, *Mater. Chem. Front.*, 2021, **5**, 3664–3672.

118 J. Zhang, W. Han, X. Zhou, X. Zhang, H. Zhang, T. Li, J. Wang, Y. Yuan, Y. He and J. Zhou, *Anal. Chem.*, 2023, **95**, 11785–11792.

119 X. Hu, Z. Fang, C. Zhu, Y. Yang, Z. Yang and W. Huang, *Adv. Funct. Mater.*, 2024, **34**, 2401325.

120 L. Xu, Q. Zhang, X. Wang and W. Lin, *Coord. Chem. Rev.*, 2024, **519**, 216122–216178.

121 T. Gong, Z. Ullah, S. Roy, C. Cheng, M. Li, J. Cheng, Y. Zhang, B. Guo and Y. Qiu, *Int. J. Nanomed.*, 2025, **20**, 9473–9503.

122 J. Liu, L. Wu, Z. Zhu, C. Yan, Y. Zhang, T. Yang, S. Xu, H. Yang, S. Liu, W. Tang, X. Ma, S. E. Lewis, Q. Wang, T. D. James and W. Zhu, *Adv. Funct. Mater.*, 2025, e15602.

12868 | *J. Mater. Chem. B*, 2025, **13**, 12831–12868

This journal is © The Royal Society of Chemistry 2025